Biomass burning aerosol over the Amazon: analysis of aircraft, surface and satellite observations using a global aerosol model

Carly L. Reddington[1], William T. Morgan[2], Eoghan Darbyshire[2], Joel Brito[3,4], Hugh Coe[2], Paulo Artaxo[3], John Marsham[1], Dominick V. Spracklen[1]

[1] School of Earth and Environment, University of Leeds, Leeds, UK.
[2] Centre of Atmospheric Sciences, School of Earth and Environmental Science, University of Manchester, Manchester, UK.
[3] Physics Institute, University of São Paulo, São Paulo, Brazil.
[4] Now at: Laboratoire de Météorologie Physique, Université Clermont Auvergne, Aubière, France.

Correspondence to: C. L. Reddington (c.l.s.reddington@leeds.ac.uk)

Abstract. Vegetation fires emit large quantities of aerosol to the atmosphere impacting regional air quality and climate. Previous work has used comparisons of simulated and observed aerosol optical depth (AOD) in regions heavily impacted by fires to suggest emissions of aerosol particles from fires may be underestimated by a factor of 2-5. Here we use surface, aircraft and satellite observations made over the Amazon during September 2012 along with a global aerosol model to improve understanding of aerosol emissions from vegetation fires. We apply three different satellite-derived fire emission datasets (FINN, GFED, GFAS) in the model. Aerosol emissions in these datasets vary by up to a factor 4 over the Amazon during this period, highlighting the considerable uncertainty in emissions. We find variable agreement between the model and observed aerosol mass concentrations. The model well reproduces observed aerosol concentrations in some periods over deforestation fires in the western Amazon. In contrast, the model underestimates aerosol concentrations over savannah fires in the eastern Amazon. The model consistently underestimates AOD compared to satellite and ground stations, even when the model reproduces the observed vertical profile of aerosol mass concentration. We suggest this is likely caused by uncertainties in the calculation of AOD, with the largest sensitivity due to uncertainty in water uptake. We therefore caution against using comparison with AOD to constrain particulate emissions from fires.

1 Introduction

Vegetation and peat fires (open biomass burning) are a major source of particulate matter (aerosol) to the atmosphere (van der Werf et al., 2010, Langmann et al., 2009) dominating the aerosol burden in many tropical regions (Lelieveld et al., 2015). There is considerable uncertainty in the magnitude of aerosol emissions from tropical fires (Reddington et al., 2016), hindering estimates of the impacts of fire on weather (Kolusu et al., 2015), climate (Rap et al., 2013; Thornhill et al., 2018) and human health (Johnston et al., 2012, Marlier et al., 2013, Reddington et al., 2015, Reid et al., 2016). Here we use the Global Model of Aerosol Processes (GLOMAP; Spracklen et al., 2005) to interpret surface, aircraft and satellite observations

made during the South American Biomass Burning Analysis (SAMBBA) field campaign during September 2012 over the Amazon basin. Our aim is to better quantify particulate emissions from fires over the Amazon basin.

Models systematically underestimate aerosol optical depth (AOD) in regions impacted by tropical biomass burning, potentially suggesting that emission datasets underestimate aerosol emissions (Reddington et al., 2016). Fire emissions

5   datasets are typically created through combining information on fire location and extent from satellite remote sensing with estimates of biomass consumption and species-specific emission factors (Langmann et al., 2009). Emissions could be underestimated due to missing fire detections or uncertainties in burned area (Randerson et al., 2012), fuel consumption (Andela et al., 2016, van Leeuwen et al., 2014), or emission factors (Stockwell et al., 2016, van Leeuwen et al., 2013). Agreement between bottom-up and top-down approaches for carbon emissions from fires is typically better than for

10   particulate matter (PM) (Yin et al., 2016), suggesting that uncertainties in burned area or fuel loads do not dominate.

Estimating emissions of PM from fires is further complicated by the emission of a range of semi-volatile and intermediate volatility organic compounds that can contribute to aerosol formation (Grieshop et al., 2009, Jathar et al., 2014). These processes are poorly understood and are not treated in many models. Observational studies report varying amounts of secondary organic aerosol (SOA) formation in different biomass burning plumes. Analysis of Siberian biomass burning

15   plumes (Konovalov et al., 2017) and southern African savannah and grassland fire plumes (Vakkari et al., 2018) show substantial in-plume SOA formation, whereas other studies report little SOA formation in tropical biomass burning plumes (Jolleys et al., 2012). At the global scale, a recent modelling study (Tsimpidi et al., 2016) estimates that 30% of organic aerosol (OA) in biomass burning aerosol originates from direct particulate emissions with the remainder being formed in the atmosphere. Analysis of OA:CO ratios in biomass burning plumes during the SAMBBA campaign suggests limited SOA

20   formation from Amazon fires (Brito et al., 2014).

Top-down studies typically use AOD, available from satellite remote sensing, to help constrain aerosol emissions from fires. In addition to particle mass concentration, simulated AOD is sensitive to assumptions about particle size, chemical composition, vertical profile of aerosol, optical properties, water uptake as well as meteorology and model resolution (Brock et al., 2016). Reddington et al. (2016) found that a global aerosol model showed better agreement with observed PM mass

25   concentration compared to AOD, potentially suggesting that some of the discrepancy between top-down and bottom up studies may be connected to the calculation of AOD.

To help explore these issues we analyse observations from the SAMBBA field campaign over the southern Amazon during the end of the dry season and transition to wet season. The Amazon exhibits a very strong seasonal cycle in aerosol concentrations (Martin et al., 2010). In the wet season PM2.5 (particulate matter with diameters smaller than 2.5 μm)

30   concentrations in the central Amazon are ~1.5 μg m^{-3} and aerosol number concentrations of 220 cm^{-3} (Poschl et al., 2010, Artaxo et al., 2013), some of the lowest concentrations observed in a terrestrial environment. In the dry season, fires occur across Southern Amazonia, resulting in aerosol concentrations that are an order of magnitude higher (PM2.5 concentrations of >30 μg m^{-3} and aerosol number concentrations > 20 000 cm^{-3} (Artaxo et al., 2013).

Fires in the Amazon are a consequence of both climate and human activity (van Marle et al., 2017). There was relatively little fire activity in the Amazon before the mid-1980s (van Marle et al., 2017), when large scale clearance of the Amazon forests began. Fire is used to clear forest and vegetation resulting in positive relationships between the rate of deforestation and fire activity in the Amazon (Aragao et al., 2008, Reddington et al., 2015, van Marle et al., 2017). A reduction in the rate

5   of deforestation across the Brazilian Amazon between 2002 and 2012 (Hansen et al., 2013) has led to reductions in deforestation-related fires (Reddington et al., 2015) and observed reductions in CO (Jiang et al., 2017) and AOD (Reddington et al., 2015). Fires are also used to maintain agricultural and pastoral land and may escape into surrounding forest leading to forest degradation (Chen et al., 2013a) and resulting in a disconnection between fire and deforestation (Aragao and Shimabukuro, 2010, Cano-Crespo et al., 2015). There has been reduction in area burned by fires in SW Amazon

10   and increase in area burned further east during the last decade (Andela et al., 2017). Droughts enhance the occurrence of fire (Chen et al., 2013b) with seasons of increased large fire occurrence coinciding with the Amazon droughts of 2005, 2007 and 2010 (Chen et al., 2013a).

Aerosol from fires degrades air quality with negative impacts on human health (Marlier et al., 2013, Reddington et al., 2015, Koplitz et al., 2016, Crippa et al., 2016). Inhalation of smoke from fires in the Amazon causes DNA damage and death of

15   human lung cells (de Oliveira Alves et al., 2017), impacts lung function (Jacobson et al., 2014), causes increased hospitalisations for respiratory diseases (Smith et al., 2014) and is estimated to result in thousands of mortalities each year (Reddington et al., 2015). Estimates on the health impacts of degraded air quality from fires require accurate information on the magnitude of particulate emissions from fire. A range of policy interventions will be necessary to reduce Amazonian fire (Morello et al., 2017).

20   Here we combine detailed observations of aerosol vertical profiles made over the Brazilian Amazon during the dry season of 2012 with surface observations, remote sensing and an aerosol model to better understand model representations of the magnitude and spatial distributions of particulate emissions from biomass burning.

2. Method

2.1 GLOMAP global aerosol model

25   We used the TOMCAT chemical transport model (Chipperfield, 2006) coupled to the GLOMAP global aerosol model (Spracklen et al., 2005) to simulate aerosol during the SAMBBA campaign. Large-scale atmospheric transport and meteorology in TOMCAT are specified from European Centre for Medium-Range Weather Forecasting (ECMWF) ERA-Interim reanalyses, updated every six hours and linearly interpolated onto the model time step. The model has a horizontal resolution of 2.8°×2.8° with 31 vertical model levels between the surface and 10 hPa. The vertical resolution in the boundary

30   layer ranges from ~60 m near the surface to ~400 m at ~2 km above the surface.

The aerosol size distribution is represented by a two-moment modal aerosol scheme (Mann et al., 2010). GLOMAP includes black carbon (BC), particulate organic matter (POM), sulfate (SO_4), sea spray and mineral dust. Concentrations of oxidants

are specified using monthly mean 3-D fields at 6-hourly intervals from a TOMCAT simulation with detailed tropospheric chemistry (Arnold et al., 2005) linearly interpolated onto the model time step.

Anthropogenic emissions of sulfur dioxide (SO_2), BC and organic carbon (OC) were specified using the MACCity emissions inventory for 2010 (Lamarque et al., 2010). Open biomass burning emissions are described in Sect. 2.2. Monthly mean

5   emissions of biogenic monoterpenes are taken from the Global Emissions InitiAtive (GEIA) database (Guenther et al., 1995). Monoterpenes are oxidised to form a product that condenses irreversibly in the particle phase (Scott et al., 2014). Size-resolved emissions of mineral dust are prescribed from daily varying emissions fluxes (Dentener et al., 2006).

2.1.1 Calculation of aerosol optical depth

AOD was calculated from the simulated aerosol size distribution as in Reddington et al. (2016), using Mie theory assuming

10   spherical particles (Grainger et al., 2004) that are internally mixed within each log-normal mode. Modelled AOD was calculated at specific wavelengths to match observations (500 nm and 550 nm), using component-specific refractive indices at the closest wavelength available from Bellouin et al. (2011).

The aerosol hygroscopicity in the AOD calculation was obtained directly from GLOMAP using the aerosol water uptake calculated online in the model using Zdanovskii-Stokes-Robinson (ZSR) theory (Stokes and Robinson, 1966) (described in

15   Sect. S1.1). We explore the sensitivity of simulated AOD to the calculation of aerosol water uptake in Sect. 3.5, by also using the κ-Köhler scheme (Petters and Kreidenweis, 2007) to calculate an offline estimate of water uptake (described in Sect. S1.2). The ZSR and κ-Köhler methods used in this study represent high and low aerosol water uptake cases, respectively (Reddington et al., 2016). In Sect. 3.5 we also explore the sensitivity of simulated AOD to assumed refractive indices and aerosol mixing state.

20   ## 2.2 Biomass burning emissions

We use three different emissions datasets of aerosol from open biomass burning: the National Centre for Atmospheric Research Fire Inventory (FINN) (Wiedinmyer et al., 2011), the Global Fire Emissions Dataset (GFED) (van der Werf et al., 2010) and the Global Fire Assimilation System (GFAS) (Kaiser et al., 2012). We use daily mean fire emissions from FINN version 1.5, GFED version 4.1s (Mu et al., 2011; van der Werf et al., 2017) and GFAS version 1.2 (hereafter referred to as

25   GFAS, FINN and GFED respectively).

Brito et al. (2014) analysed OA:CO ratios and found little enhancement of OA in fire plumes during the SAMBBA campaign, suggesting that SOA formation is limited or balanced by loss of OA through volatilization. SOA formation in plumes may be occurring on short timescales but since this was not observed in the regional-scale analysis of Brito et al. (2014), we do not include any SOA formation associated with biomass burning emissions.

30   Figure 1 compares total annual OC emissions from GFAS, FINN and GFED. The figure shows long-term (2002-2012) mean annual total emissions as well as annual total emissions in 2012, the year of the SAMBBA field campaign (total emissions

for the SAMBBA field campaign are shown in Fig. S1). For the long-term mean, all datasets show broadly similar spatial patterns with greatest OC emissions across the arc-of-deforestation (roughly 65-50°W, 8-14°S).

Table 1 compares total annual emissions from the three datasets and Figs. S3, S4 and S5 compare the total daily emissions for the 2012 dry season and the SAMBBA campaign period. FINN emissions are greater than GFED and GFAS across
5 regions of deforestation, but lower than GFED and GFAS in eastern Amazonia (50-40°W, 4-15°S). Matching 2002-2012 comparisons, FINN emissions in 2012 were also greater than GFED and GFAS over deforestation regions of western Amazonia and lower than GFED and GFAS in eastern Amazonia. Pereira et al. (2016) also reported that FINN had lower (higher) aerosol emissions in the eastern (western) Amazon compared to GFAS during the SAMBBA period. Reddington et al. (2016) reported similar patterns for comparison of GFAS version 1.0, FINN version 1.0 and GFED version 3 emissions.

10 Figure 1 also shows the difference in annual total OC emissions between 2012 and the 2002-2012 mean. All three datasets show consistently lower emissions in 2012 compared to 2002-2012 across the arc-of deforestation in western Brazil and Bolivia (70°-50°W, 8°-18°S). OC emissions in 2012 in the western Amazon were 8-45% lower than the 2002-2012 mean (Table 1). Aerosol emissions from fire in Brazil have declined over this period, related to reductions in deforestation (Reddington et al., 2015) and consistent with observed declines in CO (Jiang et al., 2017) and AOD (Reddington et al.,
15 2015). Figure S2 shows a reduction in the area dominated by deforestation type fires (and an increasing dominance of savannah-type fires) in 2012 relative to the 2002-2012 mean. In 2012, emissions were greater than the 2002-2012 average across much of Peru, possibly due to increased deforestation there (Kalamandeen et al., 2018). In the eastern Amazon, emissions in 2012 were 30-96% greater than the 2002-2012 mean (Table 1), with largest differences in GFAS and GFED datasets.

20 Fires can inject emissions above the surface due the buoyancy of the fire plume. Marenco et al. (2016) analysed Lidar data during the SAMBBA campaign and found that the mean height of aerosol layers was 2.0±0.4 km, suggesting that the majority of the aerosol is injected into the boundary layer. Fire emissions in GLOMAP are distributed vertically over six ecosystem-dependent altitudes between the surface and 6 km according to Dentener et al. (2006). Over Brazil ~53% of emissions were injected below 500 m elevation, ~30% between 500 m and 1000 m elevation, and ~17% between 1000 m
25 and 3000 m elevation. We evaluate the vertical profile of simulated aerosol in Sect. 3.2.

2.3 South American Biomass Burning Analysis (SAMBBA)

We used observations from the South American Biomass Burning Analysis (SAMBBA) campaign. Aircraft and ground observations took place from 13 September to 3 October 2012. We separate the campaign into the dry season (Phase 1; 13 to 22 September) and the dry-wet season transition (Phase 2; 22 September to 3 October) following Brito et al. (2014). Figure 3
30 shows locations of aircraft flights and surface measurement sites.

2.3.1 Aircraft observations

The BAe-146 research aircraft from the Facility for Airborne Atmospheric Measurements (FAAM) made 20 research flights with measurements of a range of gas-phase and aerosol species. We use measurements of OA and sulfate mass in the 50 - 750 nm size range from an Aerosol Mass Spectrometer (AMS) (Canagaratna et al., 2007; Morgan et al., 2010; Allan et al., 2014), refractive BC from a Single Particle Soot Photometer (SP2) (Stephens et al., 2003; McMeeking et al, 2010; Allan et al., 2014) and aerosol size distribution from a Scanning Mobility Particle Sizer (SMPS) (Wang and Flagan, 1990; Morgan et al., 2015) and a GRIMM model 1.108 optical particle counter (OPC) (Heim et al., 2008). See Allan et al. (2014) for more specific details regarding the aerosol sampling during SAMBBA.

The flights sampled a broad region spanning 46-68°W, 1-12°S (Figure 3). Aerosol properties and fire emissions (Fig. 1) varied across this region, so we separated data into a western region (53-68°W, 1-12°S) and an eastern region (43-50°W, 4.5-15°S) following Johnson et al. (2016). We used aircraft data from both vertical profiles and straight and level runs (SLR). To avoid bias, time periods when the plane was actively sampling smoke plumes were removed from the SLR data using a plume removal algorithm (Darbyshire et al., 2018). Visually observable plumes were specifically avoided when performing vertical profiles during SAMBBA so any enhancements due to smoke plumes in the profile data are small. Time periods when in-cloud sampling was performed were also filtered out of the data; specifically the data was screened for cloud artefacts when the liquid water content exceeded 0.05 g m^{-3} (Darbyshire et al., 2018).

2.3.2 Ground observations

A large suite of instruments were deployed at a site in the southwest Amazon (8.69°S, 63.87°W) (Brito et al., 2014). The site is located in a forest reserve about 5 km from Porto Velho (population of around 500 000) and is usually upwind of the city (Brito et al., 2014). Here we used measurements from an Aerosol Chemical Speciation Monitor (ACSM; Ng et al. (2011)) and an Aethalometer (Magee Scientific, model AE30). The ACSM measured 30 min resolution mass concentrations of particulate ammonium, nitrate, sulfate, chloride, and organic species in the 75 - 650 nm size range. The Aethalometer measured 5 min resolution equivalent black carbon (BC_{eq}) mass concentrations. Data from both instruments are available from the 6th September to the 1st October 2012. Mean aerosol mass concentration (ACSM + Aethalometer) during this period was 13.7 μg m^{-3}, with OA contributing an average of 83% of total mass. Mean aerosol mass concentrations were lower in Phase 2 (6.0 μg m^{-3}) compared to Phase 1 (17.8 μg m^{-3}). Full details are provided in Brito et al. (2014). PM2.5 concentrations were measured using gravimetric filter analysis, with a measurement duration ranging from less than 1 day to ~7 days (Artaxo et al., 2013).

2.3.3. AERONET aerosol optical depth

We used spectral columnar AOD measured by Aerosol Robotic Network (AERONET) Cimel sun photometers (Holben et al., 1998) from 5 stations deployed across the region that have data available for the SAMBBA campaign period: Porto

Velho UNIR (63.94°W, 8.84°S), Alta Floresta (56.10°W, 9.87°S), Rio Branco (67.87°W, 9.96°S), Cuiaba-Miranda (56.02°W, 15.73°S), Santa Cruz UTEPSA (63.20°W, 17.77°S). We used Version 3 Level 2 cloud-screened and quality assured daytime average AOD, retrieved at 500 nm. Locations of the AERONET stations are shown in Fig. 2.

2.3.4 MODIS aerosol optical depth

We used daily AOD retrieved at 550 nm from the Moderate Resolution Imaging Spectroradiometer (MODIS) instrument on board the Terra and Aqua satellites. We used the gridded 1°×1° product (Level 3 data) for the SAMBBA campaign period to calculate regional average AODs. Daytime equator crossing is 1030 for Terra and 1330 for Aqua.

2.3.5 Comparing model and observations

To compare the model to the aircraft and ground-based observations, we linearly interpolated the simulated hourly data along the flight path of the aircraft and to the horizontal location of the Porto Velho ground station. To compare with the aircraft AMS and ground-based ACSM measurements, the same detection ranges of the instruments (see Sects. 2.3.1 and 2.3.2) were applied to the simulated mass concentrations. Prior to analysis, simulated data corresponding to periods of missing measurement data were removed.

3. Results and Discussion

3.1 Surface aerosol measurements

Figure 3 shows surface PM2.5 concentrations observed at Porto Velho, in the southwest Amazon, from January to November 2012. Observed PM2.5 concentrations are less than 2 µg m^{-3} between January to July 2012, increasing to 30-50 µg m^{-3} in late August and September, then declining to less than in 10 µg m^{-3} in October. This seasonal cycle is well reproduced by the model with all fire emission datasets. Simulated PM2.5 concentrations are enhanced by biomass burning from August through to October, when more than 80% of PM2.5 concentrations are from biomass burning. PM2.5 concentrations during September are well reproduced by the model with GFED and FINN emissions, but underestimated by the model with GFAS emissions. PM2.5 concentrations are underestimated during early August, potentially indicating that emission datasets have missed fires during the start of the dry season (see Fig. S3). During the SAMBBA campaign (13 Sep – 3 Oct), PM2.5 concentrations are well reproduced by the model with FINN (r^2=0.65; normalised mean bias factor (NMBF) =0.03) and GFED (r^2=0.69; NMBF=-0.45) but underestimated with GFAS (r^2=0.44; NMBF=-1.09) (see Table 2 for a summary of NMBF values).

Figure 4 compares composition-resolved aerosol at Porto Velho during September 2012. Total aerosol mass, calculated as mass measured by the ACSM plus BC$_{eq}$ measured by the aethelometer, varies consistently with observed PM2.5 concentrations during the campaign with maximum concentrations of around 30-40 µg m^{-3} (Fig. 4a). However, total (ACSM+BC$_{eq}$) aerosol mass concentrations are consistently lower than observed PM2.5 concentrations by ~20-60% (see

Fig. S6). This difference in the observations is mostly apportioned to reduced aerosol size range from ACSM (i.e. submicrometric) in comparison to gravimetric analysis (< 2.5 µm) (Sect. 2.3.2), and, to a smaller extent, aerosol species unaccounted by the on-line instrumentation e.g. crustal elements.

Average observed total (ACSM+BC_{eq}) aerosol mass concentrations are 20 µg m^{-3} in Phase 1 reducing to 7 µg m^{-3} in Phase 2.
5   The model with fire emissions captures the decrease in observed aerosol mass concentrations between Phase 1 and Phase 2, but underestimates the magnitude of the reduction (5-10 µg m^{-3}, depending on the fire emission dataset, compared to 13 µg m^{-3} in the observations). The model with GFED simulates observed total mass well in the ACSM detection range in Phase 1 (NMBF=0.08), but overestimates observed mass in Phase 2 (NMBF=0.89). Conversely, the model with GFAS emissions simulates observed total mass reasonably well in Phase 2 (NMBF=0.30) but underestimates in Phase 1 (NMBF=-0.49). The
10   model with FINN emissions overestimates observed total mass in both Phase 1 (NMBF=0.45) and Phase 2 (NMBF=1.94).

Observed aerosol mass is dominated by OA (84%), with BC contributing 9% and summed NH_4, NO_3 and Chl contributing less than 5% of total mass during the SAMBBA campaign (Fig. 4b). Simulated aerosol (with fire emissions included) is also dominated by OA (86-88%) with BC contributing a slightly smaller fraction of the total aerosol mass (5%) than observed. NH_4, NO_3 and Chl are not accounted for in GLOMAP. Sulfate accounts for 2.6% of the observed total aerosol mass during
15   the campaign, but 5-11% in the model (Fig. 4b). Sulfate concentrations are well reproduced by the model with no fire emissions and are overestimated when fire emissions are included. This suggests that either emissions of sulfate from fires are overestimated or that other sources of sulfate are overestimated in the model.

3.2 Aerosol mass concentration vertical profile

Figure 5 compares average vertical profiles of OA, sulfate and BC measured on the aircraft to that simulated by GLOMAP.
20   As before the data is split into Phase 1 (flights 1–8) and Phase 2 (flights 9–20). We also split the data spatially into western and eastern Amazon regions (see Fig. 2). Observed aerosol concentrations are greatest in the BL then reduce rapidly above. The shape of the aerosol vertical profile is well reproduced by the model (see Fig. S7), further confirming that simulated vertical mixing and the vertical injection height of fire emissions are reasonable. Observed aerosol concentrations are relatively constant between the surface and ~2500 m in the western Amazon and between the surface and ~4000 m in the
25   eastern Amazon. This behaviour is reproduced by the model, and is likely due to a deeper BL over grassland vegetation in the eastern Amazon.

In the western Amazon, average concentrations of OA below 2.5 km (roughly the BL) were 19 µg m^{-3} in Phase 1 compared to 6 µg m^{-3} in Phase 2, similar in both magnitude and temporal pattern to the surface observations at Porto Velho. In Phase 1, the model underestimates observed OA concentrations in the BL with all emission datasets (NMBF=-0.33 for FINN to -1.96
30   for GFAS). OA concentrations in Phase 1 in the western Amazon between 3 km and 5 km are also underestimated by the model with all emission datasets consistent with comparisons in the BL. The model does not simulate the observed reduction in OA concentrations between Phase 1 and Phase 2 overestimating OA concentrations in the western Amazon in Phase 2

with GFED (NMBF=0.41) and FINN (NMBF=1.21) emissions, but good agreement with GFAS (NMBF=0.03). This may be because the emission datasets report only moderately lower emissions in Phase 2 compared to Phase 1 (Figure S4a). In the eastern Amazon, average concentrations of OA below 4 km (roughly the BL) were 16 μg m^{-3}, underestimated by the model with all three emission datasets (NMBF=-0.92 for GFAS to -2.78 for FINN).

5 Disagreement between observed and simulated OA may be due to uncertainty in the OA:OC ratio. In this study we assume an OA:OC ratio of 1.4, at the lower end of the range (1.4 to 2.6) assumed by other models (Tsigaridis et al., 2014). Philip et al. (2014) combined satellite data and AMS measurements to estimate an OA:OC ratio of 1.3 to 2.1. Preliminary analysis of aircraft data during SAMBBA suggests an OA:OC ratio of 1.5 to 1.8 for fresh BB aerosol and 2.0 to 2.3 for aged aerosol (Johnson et al., 2016). Assuming an OA:OC ratio of 2.3 would enhance our simulated OA concentrations by 60% reducing
10 our underestimate of OA in both the western (NMBF=-0.85 to 0.20) and eastern (NMBF=-1.36 to -0.20) Amazon.

Observed refractive BC (rBC) concentrations in the BL are ~1.0 μg m^{-3} in the western Amazon during Phase 1 dropping to ~0.5 μg m^{-3} in during Phase 2. BC concentrations observed at the surface (Sect. 3.1; Phase 1, 1.6 μg m^{-3}; Phase 2, 0.9 μg m^{-3}) are greater than those measured on the aircraft, although this may be partly due to the different measurement techniques used and different size detection ranges. In the eastern Amazon, observed rBC concentrations are higher (1.8 μg m^{-3}), qualitatively
15 reproduced by the model with GFAS and GFED emissions but not with FINN emissions. The model strongly underestimates BC concentrations in the eastern Amazon with all emission datasets, particularly with FINN (NMBF=-1.41 for GFAS to -5.55 for FINN). In the west the agreement is more variable, with the model well simulating concentrations in Phase 1 with FINN emissions but overestimating in Phase 2, GFED underestimating in Phase 1 but well simulating concentrations in Phase 2 and the model with GFAS emissions underestimating in both phases.

20 In the western Amazon, comparison with sulfate aerosol is fairly consistent with OA and BC comparisons, with the model underestimating in Phase 1 and overestimating in Phase 2. In the eastern Amazon, the model overestimates sulfate concentrations even without a contribution from fires, suggesting that other natural and anthropogenic sulfate sources are overestimated in the model.

Observed average BC:OA mass concentration ratios in the BL vary from 0.05 in the western Amazon (Phase 1, 1/19=0.05;
25 Phase 2, 0.5/6=0.08) to 0.11 (1.8/16=0.11) in the eastern Amazon. These ratios reflect the much higher BC emission factors found for fires in the eastern Amazon relative to fires in the western Amazon (Hodgson et al., 2018). Simulated ratios are in good agreement with observations in the western Amazon with all emission datasets (e.g. Phase 1, FINN: 1/14=0.07; Phase 2, FINN: 0.8/13=0.06). In the eastern Amazon, BC:OC ratios are underestimated using FINN (0.3/4.2=0.07) emissions, with better agreement using GFED (0.7/7.5=0.09) and GFAS (0.8/8.2=0.10) emissions.

30 In the western Amazon, average aerosol concentrations at 4 km are ~27-50% of concentrations in the BL (<2.5 km) (OA$_{P1}$: 7/19=0.37, OA$_{P2}$: 3/6=0.50; BC$_{P1}$: 0.27/1=0.27, BC$_{P2}$: 0.26/0.5=0.52). Marenco et al. (2016) reported a mean aerosol layer of 2.0±0.4 km during the SAMBBA campaign, which is consistent with the model results presented here. A plume-rise model coupled to WRF-Chem overestimated OA concentrations at 6-8 km altitude observed over tropical forest regions during

SAMBBA, suggesting the plume rise model overestimated fire injection height (Archer-Nicholls et al., 2015). Overall there appears to be limited evidence for the need for substantial injection of fire emissions above the BL for fires in this region.

Overall, the comparisons with aircraft observations show variable agreement between model and observations. The model with GFAS emissions consistently underestimates observed aerosol mass concentrations by up to a factor 3, but gives the

5 best agreement (relative to GFED and FINN) with observations in the eastern Amazon. Agreement between the model and observations with GFED and FINN emissions is more variable with up to a factor 2-3 underestimation or overestimation, depending on the region and time period. In general, the model with FINN emissions performs well against observations in the western Amazon in Phase 1 (when observed aerosol mass concentrations are relatively high), but gives the largest underestimation of aerosol mass concentrations in the eastern Amazon (relative to GFED and GFAS).

10 **3.3 Aerosol size distribution**

Figure 6 compares simulated aerosol size distributions against those measured on the aircraft during straight and level runs. In the eastern Amazon, the model underestimates particle number below 300 nm diameter, consistent with aerosol mass comparisons (Sect. 3.2). In the western Amazon, the model with FINN and GFED emissions generally well matches the observed size distribution above 200 nm diameter, with a small underestimate during Phase 1 consistent with the vertical

15 profiles of aerosol mass (Fig. 5). The model with GFAS emissions underestimates throughout the size distribution, consistent with earlier comparisons.

There is a persistent underestimation of aerosol number at particle sizes below about 100 nm. We assume all biomass burning emissions are emitted into the accumulation mode with geometric mean diameter of 150 nm (Mann et al., 2010), which is substantially higher than observed in the ground station data (94 nm; Brito et al., 2014). The observations suggest

20 biomass burning makes a considerable contribution to aerosol number from ~50 to 200 nm diameter that is not included in the model. This is consistent with Vakkari et al. (2018), where assumed emission size distributions in models poorly represented the number of particles in the 30–100 nm (Aitken mode) size range for southern African savannah and grassland fires. The particle number in the Aitken mode size range will have a negligible effect on AOD but may be important for cloud condensation nuclei concentrations.

25 **3.4 Aerosol optical depth**

Figure 7 compares simulated and satellite-retrieved (MODIS) AOD at 550 nm (AOD550) over the eastern and western regions for the SAMBBA campaign period. Compared to MODIS, the model consistently underestimates AOD over both regions and with all fire emission datasets (see NMBF in Table 3). The model with GFAS emissions has the largest underestimation in the western Amazon (the smallest with FINN) and the model with FINN emissions has the largest

30 underestimate in the eastern Amazon (the smallest with GFAS). The model with FINN emissions underestimates AOD in the western Amazon in Phase 2 even when it overestimates aerosol mass concentrations throughout the vertical profile. In the

eastern region, the underestimation of AOD with all emission datasets is consistent with the comparison of the vertical profile of aerosol mass concentration.

Figure 8 compares simulated and observed AOD at 500 nm (AOD500) at five AERONET sites across western and southern Amazonia during SAMBBA (no data is available from the AERONET station located in the eastern region during the campaign). There is reasonable agreement between AOD500 reported by AERONET and AOD550 reported by MODIS, with AERONET generally reporting higher values (Aqua, NMBF=-0.60 to -0.27; Terra, NMBF=-0.47 to -0.18). Consistent with comparisons to MODIS, the model consistently underestimates AOD500 at all stations and with all fire emissions, except at Rio Branco in the western Amazon with FINN emissions. For all stations, the model with GFAS emissions has the largest underestimation (Table 3). The fire emission dataset that gives the smallest model bias varies between GFED and FINN depending on the station and time period (Phase 1 or 2 of the campaign; Table 3). The smallest model underestimate for all simulations is at Rio Branco in the western Amazon (e.g. with FINN: $NMBF_{P1} = 0.03$, $NMBF_{P2} = 0.11$).

The model consistently underestimates observed AOD during the SAMBBA campaign despite relatively good agreement with observed aerosol size distribution (> 200 nm diameter) and aerosol mass concentrations at the surface (consistent with Reddington et al. (2016)) and aloft in the western Amazon region. The calculation of AOD also depends on aerosol optics and water uptake. We explore the sensitivity of simulated AOD to these other factors in the following section.

3.5 Exploring the sensitivity of simulated aerosol optical depth

In Reddington et al. (2016) we identified a greater model underestimation of AOD than surface PM2.5 in the Amazon region, where coincident observations were available, suggesting that the negative model bias in AOD could be caused by errors in the calculation of AOD rather than by errors in simulated aerosol properties. However, due to a lack of available observations, we were unable to rule out errors in simulated aerosol size distribution and vertical profile (i.e. an underestimation of aerosol aloft) with any certainty.

In this work, using the detailed SAMBBA observations, we have shown that the model well represents the vertical profile of aerosol mass concentrations and aerosol size distribution (in the diameter range relevant for visible light) in the western Amazon, yet continues to underestimate AOD. Below we explore the sensitivity of simulated AOD to other relevant aerosol properties including aerosol mixing state, refractive indices and hygroscopicity.

3.5.1 Mixing state

We find that simulated AOD is relatively insensitive to the assumption about the aerosol mixing state; with less than 5% difference in the magnitude of AOD between internally mixed and externally mixed cases (consistent with Reddington et al., 2016). Calculating AOD assuming optical properties derived from an external mixture of aerosol species leads to slightly reduced values (by ~1-4%) when compared to AOD calculated assuming an internal (volumetrically-averaged) aerosol mixture. Han et al. (2013) also find relatively small changes in the magnitude of AOD (0.03 to 0.07) in high AOD regions

(~0.8 to 2.0) between internally and externally mixed cases, with the internal mixture assumption giving higher values than the external mixture assumption.

Curci et al. (2015) find a greater difference (~37%) in simulated AOD between internally and externally mixed assumptions, with the external mixed case giving the highest AOD. However, the greater sensitivity of simulated AOD to the mixing state assumption in Curci et al. (2015) was chiefly due to the difference in the calculation of the aerosol number size distribution rather than the difference in the calculated optical properties. The GLOMAP model simulates both mass and number concentration of each size mode so the total number concentration stays identical for both mixing state assumptions (in the externally mixed case the number concentration of particles in a given size mode is split between aerosol components based on the volume fraction of that component in the mode). We note that the internally mixed case used in this study does not consider different mixing structure assumptions i.e. core-shell internal mixing, which may account for an additional uncertainty of ~5-10% in simulated AOD (Curci et al., 2015).

3.5.2 Refractive index

To investigate the sensitivity of simulated AOD to assumptions about the aerosol optical properties, we calculated AOD550 from the model simulation with GFED emissions assuming a range of refractive indices appropriate for BC and POM aerosol (see Table S1). We find that the magnitude of simulated AOD550 varies by up to ~8% (relative to the control AOD) depending on the choice of refractive indices.

Applying smoke aerosol refractive indices from Matichuk et al. (2007; 2008) to the model BC and POM components leads to a small mean decrease in AOD550 relative to the control (by 2-5% in the eastern region and 0-3% in the western region; Table S1). Assuming medium and highly absorbing refractive indices for BC from Bond and Bergstrom (2006) increases AOD550 by an average of 4-6% in the eastern region and 2-3% in the western region. Using the highly absorbing refractive index for BC gives the best agreement between model and satellite-retrieved (MODIS) AOD550 (Table S1).

The relatively small sensitivity of simulated AOD to assumed aerosol refractive indices is consistent with previous studies (Matichuk et al., 2007; Curci et al., 2015; Reddington et al., 2016) and suggests that the negative bias in AOD cannot be wholly explained by the uncertainty associated with this assumption.

3.5.3 Aerosol water uptake and relative humidity

Aerosol water uptake plays a significant role in determining AOD, altering the refractive index and the size distribution of the aerosol. Our estimate of aerosol water uptake depends on the calculation method (including assumptions made regarding aerosol hygroscopicity; described in Sects. 2.1.1 and S1), the model relative humidity (from ECMWF reanalyses) and the simulated aerosol physical/chemical properties (size distribution and composition).

To test the sensitivity of AOD to the calculation of aerosol water uptake, we compare AOD550 calculated using two methods (described in S1): 1) using ZSR online in the model and 2) using the κ-Köhler water uptake scheme (Petters and

Kreidenweis, 2007) offline during post-processing. Our previous work demonstrated that simulated AOD is sensitive to this calculation, with simulated AOD440 varying by a factor of ~1.6 between the upper and lower estimates of water uptake (Reddington et al., 2016). We find the same here, with AOD550 varying by a mean factor of 1.6 over the western Amazon and a mean factor of 1.5 over the eastern Amazon, between the two calculation methods. Using the κ-Köhler water uptake

5   scheme decreases AOD550 (by 32-38%) relative to AOD550 calculated using ZSR, thus increasing the negative model bias against observations.

In Reddington et al. (2016) we discussed the potential sensitivity of simulated AOD to errors in relative humidity. In this work we are able to evaluate the model relative humidity against SAMBBA aircraft observations. Figure S8 shows average vertical profiles of simulated and observed relative humidity during the SAMBBA campaign. The model captures the shape

10   of the profile of observed relative humidity in both western and eastern regions (NMBF=-0.03); with small over/underestimates in the BL in the western/eastern regions, respectively (western BL: NMBF=0.10; eastern BL: NMBF=-0.05). These results suggest that model relative humidity is unlikely to be responsible for the negative bias in AOD, since higher model relative humidity in the western region will act to increase AOD due to more water uptake by the aerosol.

3.5.4 Model spatial resolution

15   It is important to mention that the relatively coarse spatial resolution of the simulated aerosol and relative humidity fields may also contribute to the model underestimation of AOD. Increasing model spatial resolution has been shown to increase simulated AOD by ~11-13% (Bian et al., 2009; Weigum et al., 2016), depending on the initial and altered grid resolutions. Increasing simulated AOD by ~13% would improve agreement between model and observations but not fully resolve the negative bias in model AOD. Furthermore, comparisons between simulated and aircraft observed aerosol mass

20   concentrations and relative humidity suggest that the model captures observed spatial variations in aerosol mass concentrations reasonably well for the SAMBBA period, at least over the western Amazon region. A higher resolution model would be required to explore the degree of sensitivity of AOD to the spatial resolution of simulated aerosol and relative humidity fields in detail.

4. Conclusions

25   We have used surface, aircraft and satellite observations made during the SAMBBA field campaign in the southern Amazon during September and October 2012 to improve our understanding of biomass burning emissions. We apply three different biomass burning emission datasets (FINN, GFAS, GFED) in the GLOMAP global aerosol model. Total annual aerosol emissions from fires across the Amazon region vary by up to a factor 3.7 across these datasets, highlighting the large uncertainty in aerosol emissions from fires. In 2012, annual aerosol fire emissions were 8-45% less than the 2002-2012 mean

30   in the western Amazon, but 30-94% greater than the long-term mean in the eastern Amazon. This reflects declining

deforestation rate and associated fires in the western Amazon over this period (Redddington et al., 2015) and opposing trends in fires in the eastern Amazon (Andela et al, 2018).

During 2012, observed surface PM2.5 concentrations in the southern Amazon increased from ~2 μg m^{-3} between January and July to 30-50 μg m^{-3} in September then declined to less than 10 μg m^{-3} in October. Observed aerosol mass (in the 75 - 650 nm diameter size range) in September was dominated by OA which accounted for 84% of total mass with BC accounting for 9% of mass. The model reproduced the observed seasonal cycle of aerosol concentrations, with ~54-78% of simulated PM2.5 concentrations originating from fire emissions during September 2012. Fires are the dominant source of PM2.5 across the region during the dry season.

In the western Amazon, where deforestation fires are the dominant fire type, agreement between simulated and observed aerosol mass concentrations in the BL is variable, depending on the fire emission dataset used both for OA (NMBF = -1.96 to +1.21) and BC (NMBF=-1.32 to +0.56). In this region we do not find evidence that aerosol emissions are systematically underestimated across all emission datasets. In the eastern Amazon, where grassland/savannah fires are dominant, GLOMAP underestimates OA (NMBF = -0.9 to -2.8) and BC (NMBF = -1.4 to -5.6) concentrations with all three emission datasets. This suggests that all emission datasets may underestimate aerosol emissions from grassland/savannah fires in the eastern Amazon. We assume fire emissions have an OA:OC ratio of 1.4. Increasing our OA:OC ratio to 2.3, towards the upper end of that used in models (Tsigaridis et al., 2014) and matching aged aerosol observed in SAMBBA (Johnson et al., 2016), would improve the model-observation OA comparison in the eastern Amazon but would lead to an overestimate of OA in the western Amazon in some periods.

Observed vertical profiles of aerosol mass concentrations were characterised by enhanced concentrations from the surface up to around 2 km altitude in the western Amazon and 4 km altitude in the eastern Amazon. In our model, we assume that all emissions from vegetation fires in this region are injected below 3 km altitude, with ~80% of emissions injected below 1 km. The model simulated a realistic relative vertical profile of aerosol mass concentrations, suggesting that our assumptions about injection height are valid. This further confirms that Amazon fires rarely inject emissions above the BL, as found by previous studies (Archer-Nicholls et al., 2015, Marenco et al., 2016).

The model systematically underestimates AOD across the Amazon both in comparison to AERONET (NMBF=-1.31 to -0.43) and MODIS (NMBF =-2.41 to -0.96). In the Eastern Amazon the underestimation of aerosol mass concentrations through the vertical profile contributes to this underestimation of AOD. In the western Amazon, the model underestimates AOD even when the vertical profile of aerosol mass concentration is either well predicted or overestimated. This suggests that underestimation of AOD may be due to uncertainties in the calculation of AOD, rather than underestimation of aerosol mass concentrations. To explore this possibility we tested the impact of uncertainty in refractive index, aerosol mixing state and aerosol water uptake on calculated AOD. We found that simulated AOD was most sensitive to assumptions about water uptake.

Overall, our work suggests that aerosol emissions from fires are on average underestimated over the Amazon, particularly over grassland fires in the eastern Amazon, albeit by less than the factor 3-5 assumed in some previous studies. Confirming our previous work (Reddington et al., 2016) we find that simulated and observed aerosol mass concentrations are generally in better agreement than simulated and observed AOD. We show that the model underestimates AOD even when it reproduces the observed vertical profile of aerosol mass. This suggests that uncertainties in the calculation of AOD, rather than the aerosol mass concentration, are the dominant reason for underestimation of AOD, and we find largest sensitivity to uncertainty in water uptake. We therefore caution against using comparison with AOD to scale particulate emissions from fires, as has been done in a number of previous studies.

Acknowledgements. This research was supported by funding from the Natural Environment Research Council for the South American Biomass Burning Analysis (SAMBBA) project (number NE/J009822/1). The authors gratefully acknowledge the principal investigators (B. Holben and P. Artaxo) and their staff responsible for establishing and maintaining the five AERONET stations used in this study and providing quality-assured data.

References

Allan, J. D., Morgan, W. T., Darbyshire, E., Flynn, M. J., Williams, P. I., Oram, D. E., Artaxo, P., Brito, J., Lee, J. D., and Coe, H.: Airborne observations of IEPOX-derived isoprene SOA in the Amazon during SAMBBA, Atmos. Chem. Phys., 14, 11393-11407, https://doi.org/10.5194/acp-14-11393-2014, 2014.

Andela, N., van der Werf, G. R., Kaiser, J. W., van Leeuwen, T. T., Wooster, M. J., and Lehmann, C. E. R.: Biomass burning fuel consumption dynamics in the tropics and subtropics assessed from satellite, Biogeosciences, 13, 3717-3734, https://doi.org/10.5194/bg-13-3717-2016, 2016.

Andela, N., Morton, D. C., Giglio, L., Chen, Y., van der Werf, G. R., Kasibhatla, P. S., DeFries, R. S., Collatz, G. J., Hantson, S., Kloster, S., Bachelet, D., Forrest, M., Lasslop, G., Li, F., Mangeon, S., Melton, J. R., Yue, C. and Randerson, J. T.: A human-driven decline in global burned area, Science, 356, 1356-1361, 2017.

Aragao, L., Malhi, Y., Barbier, N., Lima, A., Shimabukuro, Y., Anderson, L. and Saatchi, S.: Interactions between rainfall, deforestation and fires during recent years in the Brazilian Amazonia, Philosophical Transactions of the Royal Society B-Biological Sciences, 363, 1779-1785, 2008.

Aragao, L. and Shimabukuro, Y. E.: The Incidence of Fire in Amazonian Forests with Implications for REDD, Science, 328, 1275-1278, 2010.

Archer-Nicholls, S., Lowe, D., Darbyshire, E., Morgan, W. T., Bela, M. M., Pereira, G., Trembath, J., Kaiser, J. W., Longo, K. M., Freitas, S. R., Coe, H., and McFiggans, G.: Characterising Brazilian biomass burning emissions using WRF-Chem with MOSAIC sectional aerosol, Geosci. Model Dev., 8, 549-577, https://doi.org/10.5194/gmd-8-549-2015, 2015.

Arnold, S. R., Chipperfield, M. P., and Blitz, M. A.: A three dimensional model study of the effect of new temperature dependent quantum yields for acetone photolysis, J. Geophys. Res., 110, D22305, doi:10.1029/2005JD005998, 2005.

Artaxo, P., Rizzo, L. V., Brito, J. F., Barbosa, H. M. J., Arana, A., Sena, E. T., Cirino, G. G., Bastos, W., Martin, S. T., and Andreae, M. O.: Atmospheric aerosols in Amazonia and land use change: From natural biogenic to biomass burning conditions, Faraday Discuss., 165, 203-235, 2013.

Bian, H., Chin, M., Rodriguez, J. M., Yu, H., Penner, J. E., and Strahan, S.: Sensitivity of aerosol optical thickness and aerosol direct radiative effect to relative humidity, Atmos. Chem. Phys., 9, 2375-2386, doi:10.5194/acp-9-2375-2009, 2009.

Bellouin, N., Rae, J., Jones, A. Johnson, C., Haywood, J. and Boucher, O.: Aerosol forcing in the Climate Model Intercomparison Project (CMIP5) simulations by HadGEM2-ES and the role of ammonium nitrate, J. Geophys. Res., 116, D20206, doi:10.1029/2011JD016074, 2011.

Bond, T. C. and Bergstrom, R. W.: Light absorption by carbonaceous particles: An investigative review, Aerosol Sci. Technol., 40, 27-67, 2006.

Brito, J., Rizzo, L. V., Morgan, W. T., Coe, H., Johnson, B., Haywood, J., Longo, K., Freitas, S., Andreae, M. O., and Artaxo, P.: Ground-based aerosol characterization during the South American Biomass Burning Analysis (SAMBBA) field experiment, Atmos. Chem. Phys., 14, 12069-12083, doi:10.5194/acp-14-12069-2014, 2014.

Brock, C. A., Wagner, N. L., Anderson, B. E., Beyersdorf, A., Campuzano-Jost, P., Day, D. A., Diskin, G. S., Gordon, T. D., Jimenez, J. L., Lack, D. A., Liao, J., Markovic, M. Z., Middlebrook, A. M., Perring, A. E., Richardson, M. S., Schwarz, J. P., Welti, A., Ziemba, L. D., and Murphy, D. M.: Aerosol optical properties in the southeastern United States in summer – Part 2: Sensitivity of aerosol optical depth to relative humidity and aerosol parameters, Atmos. Chem. Phys., 16, 5009-5019, https://doi.org/10.5194/acp-16-5009-2016, 2016.

Cano-Crespo, A., P. J. C. Oliveira, A. Boit, M. Cardoso, and K. Thonicke: Forest edge burning in the Brazilian Amazon promoted by escaping fires from managed pastures, J. Geophys. Res. Biogeosci., 120, 2095–2107, doi: 10.1002/2015JG002914, 2015.

Canagaratna, M. R., Jayne, J. T., Jimenez, J. L., Allan, J. D., Alfarra, M. R., Zhang, Q., Onasch, T. B., Drewnick, F., Coe, H., Middlebrook, A., Delia, A., Williams, L. R., Trimborn, A. M., Northway, M. J., DeCarlo, P. F., Kolb, C. E., Davidovits, P., and Worsnop, D. R.: Chemical and microphysical characterization of ambient aerosols with the aerodyne aerosol mass spectrometer, Mass Spectrom. Rev., 26, 185–222, https://doi.org/10.1002/mas.20115, 2007.

Channan, S., Collins, K. and Emanuel, W. R.: Global mosaics of the standard MODIS land cover type data. University of Maryland and the Pacific Northwest National Laboratory, College Park, Maryland, USA, 2014.

Chen, Y., Morton, D. C., Jin, Y. F., Collatz, G. J., Kasibhatla, P. S., van der Werf, G. R., DeFries, R. S. & Randerson, J. T.: Long-term trends and interannual variability of forest, savanna and agricultural fires in South America, Carbon Management, 4, 617-638, doi: 10.4155/cmt.13.61 2013a.

Chen, Y., I. Velicogna, J. S. Famiglietti, and J. T. Randerson: Satellite observations of terrestrial water storage provide early warning information about drought and fire season severity in the Amazon, J. Geophys. Res. Biogeosci., 118, 495–504, doi: 10.1002/jgrg.20046, 2013b.

Chipperfield, M. P.: New version of the TOMCAT/SLIMCAT off-line chemical transport model: Intercomparison of stratospheric tracer experiments, Q. J. Royal Meteorol. Soc., 132, 1179-1203, 2006.

Crippa, P., Castruccio, S., Archer-Nicholls, S., Lebron, G. B., Kuwata, M., Thota, A., Sumin, S., Butt, E., Wiedinmyer, C. and Spracklen, D. V.: Population exposure to hazardous air quality due to the 2015 fires in Equatorial Asia, Sci. Rep., 6, 37074, 2016.

Curci, G., Hogrefe, C., Bianconi, R., Im, U., Balzarini, A., Baro, R., Brunner, D., Forkel, R., Giordano, L., Hirtl, M., Honzak, L., Jimenez-Guerrero, P., Knote, C., Langer, M., Makar, P., Pirovano, G., Perez, J.L., San Jose, R., Syrakov, D., Tuccella, P., Werhahn, J., Wolke, R., Zabkar, R. and Zhang, J.: Uncertainties of simulated aerosol optical properties induced by assumptions on aerosol physical and chemical properties: an AQMEII-2 perspective, Atmos. Environ, 115, 541-552, 2015.

Darbyshire, E., Morgan, W. T., Allan, J. D., Liu, D., Flynn, M. J., Dorsey, J. R., O'Shea, S. J., Lowe, D., Szpek, K., Marenco, F., Johnson, B. T., Bauguitte, S., Haywood, J. M., Brito, J. F., Artaxo, P. E., Longo, K. M., & Coe, H.: The vertical distribution of biomass burning pollution over tropical South America from aircraft in-situ measurements during SAMBBA, in preparation, 2018.

5 de Oliveira Alves, N., Vessoni, A. T., Quinet, A., Fortunato, R. S., Kajitani, G. S., Peixoto, M. S., Hacon, S. D., Artaxo, P., Saldiva, P., Menck, C. F. M. and Batistuzzo de Medeiros, S. R.: Biomass burning in the Amazon region causes DNA damage and cell death in human lung cells, Sci. Rep., 7, 13, 2017.

Dentener, F., Kinne, S., Bond, T., Boucher, O., Cofala, J., Generoso, S., Ginoux, P., Gong, S., Hoelzemann, J.J., Ito, A., Marelli, L., Penner, J.E., Putaud, J.-P., Textor, C., Schulz, M., van der Werf, G.R., and Wilson, J.: Emissions of
10   primary aerosol and precursor gases in the years 2000 and 1750 prescribed data-sets for AeroCom, Atmos. Chem. Phys., 6, 4321–4344, doi:10.5194/acp-6-4321-2006, 2006.

Friedl, M.A., Sulla-Menashe, D., Tan, B., Schneider, A., Ramankutty, N., Sibley, A., and Huang, X.: MODIS Collection 5 global land cover: Algorithm refinements and characterization of new datasets, 2001-2012, Collection 5.1 IGBP Land Cover, Boston University, Boston, MA, USA, 2010.

15 Grainger, R. G., Lucas, J., Thomas, G. E., and Ewen, G. B. L.: Calculation of Mie Derivatives, Appl. Opt., 43, 5386, doi:10.1364/AO.43.005386, 2004.

Grieshop, A. P., Logue, J. M., Donahue, N. M., and Robinson, A. L.: Laboratory investigation of photochemical oxidation of organic aerosol from wood fires 1: measurement and simulation of organic aerosol evolution, Atmos. Chem. Phys., 9, 1263-1277, https://doi.org/10.5194/acp-9-1263-2009, 2009.

20 Han, X., Zhang, M.G., Zhu, L.Y. and Xu, L.R.: Model analysis of influences of aerosol mixing state upon its optical properties in East Asia, Adv. Atmos. Sci., 30, 1201–1212, 2013.

Hansen, M. C., Potapov, P. V.,Moore, R., Hancher, M., Turubanova, S. A., Tyukavina, A.,Thau, D., Stehman, S. V., Goetz, S. J., Loveland, T. R.,Kommareddy, A., Egorov, A., Chini, L., Justice, C. O. and Townshend, J. R. G.: High-Resolution Global Maps of 21st-Century Forest Cover Change, Science, 342, 850-853, 2013.

25 Heim, M., Mullins, B. J., Umhauer, H. & Kasper, G.: Performance evaluation of three optical particle counters with an efficient "multimodal" calibration method, J. Aerosol Sci., 39(12), 1019–1031, doi:10.1016/j.jaerosci.2008.07.006, 2008.

Hodgson, A. K., Morgan, W. T., O'Shea, S., Bauguitte, S., Allan, J. D., Darbyshire, E., Flynn, M. J., Liu, D., Lee, J., Johnson, B., Haywood, J. M., Longo, K. M., Artaxo, P. E., and Coe, H.: Near-field emission profiling of tropical
30   forest and Cerrado fires in Brazil during SAMBBA 2012, Atmos. Chem. Phys., 18, 5619-5638, https://doi.org/10.5194/acp-18-5619-2018, 2018.

Holben, B. N., Eck, T. F., Slutsker, I., Tanré, D., Buis, J. P., Setzer, A., Vermote, E., Reagan, J. A., Kaufman, Y. J., Nakajima, T., Lavenu, F., Jankowiak, I., and Smirnov, A.: AERONET—A Federated Instrument Network and Data Archive for Aerosol Characterization, Remote Sens. Environ., 66, 1, 1-16, http://dx.doi.org/10.1016/S0034-
35   4257(98)00031-5, 1998.

Jacobson, L.d.S.V., Hacon, S.d.S., Castro, H.A.d., Ignotti, E., Artaxo, P., Saldiva, P.H.N., Leon, A.C.M. P.d.: Acute effects of particulate matter and black carbon from seasonal fires on peak expiratory flow of schoolchildren in the Brazilian Amazon, Plos One, 9(8): e104177, doi:10.1371/journal.pone.0104177, 2014.

Jathar, S. H., Gordon, T. D., Hennigan, C. J., Pye, H. O. T., Pouliot, G., Adams, P. J., Donahue, N. M. and Robinson, A. L.:
40   Unspeciated organic emissions from combustion sources and their influence on the secondary organic aerosol budget in the United States, Proc. Natl. Acad. Sci. USA, 111, 10473-10478, 2014.

Jiang, Z., Worden, J. R., Worden, H., Deeter, M., Jones, D. B. A., Arellano, A. F., and Henze, D. K.: A 15-year record of CO emissions constrained by MOPITT CO observations, Atmos. Chem. Phys., 17, 4565-4583, https://doi.org/10.5194/acp-17-4565-2017, 2017.

Johnson, B. T., Haywood, J. M., Langridge, J. M., Darbyshire, E., Morgan, W. T., Szpek, K., Brooke, J. K., Marenco, F., Coe, H., Artaxo, P., Longo, K. M., Mulcahy, J. P., Mann, G. W., Dalvi, M., and Bellouin, N.: Evaluation of biomass burning aerosols in the HadGEM3 climate model with observations from the SAMBBA field campaign, Atmos. Chem. Phys., 16, 14657-14685, https://doi.org/10.5194/acp-16-14657-2016, 2016.

Johnston, F. H., Henderson, S. B., Chen, Y., Randerson, J. T., Marlier, M., Defries, R. S., Kinney, P., Bowman, D. M. and Brauer, M.: Estimated global mortality attributable to smoke from landscape fires, Environ. Health Perspect., 120, 695-701, 2012.

Jolleys, M. D., Coe, H., McFiggans, G., Capes, G., Allan, J. D., Crosier, J., Williams, P. I., Allen, G., Allen, K. N., Jimenez, J. L., Russell, L. M., Grutter, M. and Baumgardner, D.: Characterizing the Aging of Biomass Burning Organic Aerosol by Use of Mixing Ratios: A Meta-analysis of Four Regions, Environ. Sci. Technol., 46, 13093-13102, 2012.

Kaiser, J. W., Heil, A., Andreae, M. O., Benedetti, A., Chubarova, N., Jones, L., Morcrette, J.-J., Razinger, M., Schultz, M. G., Suttie, M., and van der Werf, G. R.: Biomass burning emissions estimated with a global fire assimilation system based on observations of fire radiative power, Biogeosciences, 9, 527-554, doi:10.5194/bg-9-527-2012, 2012.

Kalamandeen, M., Gloor, E., Mitchard, E., Quincey, D., Ziv, G., Spracklen, D., Spracklen, B., Adami, M., Aragao, L. and Galbraith, D.: Pervasive Rise of Small-scale Deforestation in Amazonia, Sci. Rep., 8, 10, 2018.

Kolusu, S. R., Marsham, J. H., Mulcahy, J., Johnson, B., Dunning, C., Bush, M., and Spracklen, D. V.: Impacts of Amazonia biomass burning aerosols assessed from short-range weather forecasts, Atmos. Chem. Phys., 15, 12251-12266, doi:10.5194/acp-15-12251-2015, 2015.

Konovalov, I. B., Beekmann, M., Berezin, E. V., Formenti, P., and Andreae, M. O.: Probing into the aging dynamics of biomass burning aerosol by using satellite measurements of aerosol optical depth and carbon monoxide, Atmos. Chem. Phys., 17, 4513-4537, https://doi.org/10.5194/acp-17-4513-2017, 2017.

Koplitz, S. N., Mickley, L. J., Marlier, M. E., Buonocore, J. J., Kim, P. S., Liu, T. J., Sulprizio, M. P., DeFries, R. S., Jacob, D. J., Schwartz, J., Pongsiri, M. and Myers, S. S.: Public health impacts of the severe haze in Equatorial Asia in September-October 2015: demonstration of a new framework for informing fire management strategies to reduce downwind smoke exposure, Environ. Res. Lett., 11, 10, 2016.

Lamarque, J.-F., Bond, T. C., Eyring, V., Granier, C., Heil, A., Klimont, Z., Lee, D., Liousse, D., Mieville, A., Owen, B., Schultz, M. G., Shindell, D., Smith, S. J., Stehfest, E., Van Aardenne, J., Cooper, O. R., Kainuma, M., Mahowald, N., McConnell, J. R., Naik, V., Riahi, K., and van Vuuren, D. P.: Historical (1850-2000) gridded anthropogenic and biomass burning emissions of ozone and aerosol precursors: methodology and application, Atmos. Chem. Phys., 10, 7017-7039, doi:10.5194/acp-10-7017-2010, 2010.

Langmann, B., Duncan, B., Textor, C., Trentmann, J. and van der Werf, G. R.: Vegetation fire emissions and their impact on air pollution and climate, Atmos. Environ., 43, 107-116, 2009.

Lelieveld, J., Evans, J. S., Fnais, M., Giannadaki, D. and Pozzer, A.: The contribution of outdoor air pollution sources to premature mortality on a global scale, Nature, 525, 367, 2015.

Mann, G. W., Carslaw, K. S., Spracklen, D. V., Ridley, D. A., Manktelow, P. T., Chipperfield, M. P., Pickering, S. J., and Johnson, C. E.: Description and evaluation of GLOMAP-mode: a modal global aerosol microphysics model for the UKCA composition-climate model, Geosci. Model Dev., 3, 519-551, doi:10.5194/gmd-3-519-2010, 2010.

Marenco, F., Johnson, B., Langridge, J. M., Mulcahy, J., Benedetti, A., Remy, S., Jones, L., Szpek, K., Haywood, J., Longo, K., and Artaxo, P.: On the vertical distribution of smoke in the Amazonian atmosphere during the dry season, Atmos. Chem. Phys., 16, 2155-2174, https://doi.org/10.5194/acp-16-2155-2016, 2016.

Marlier, M. E., DeFries, R. S., Voulgarakis, A., Kinney, P. L., Randerson, J. T., Shindell, D. T., Chen, Y. and Faluvegi, G.: El Niño and health risks from landscape fire emissions in southeast Asia, Nature Clim. Change, 3, 131-136, doi:10.1038/nclimate1658, 2013.

Martin, S. T., Andreae, M. O., Artaxo, P., Baumgardner, D., Chen, Q., Goldstein, A. H., Guenther, A., Heald, C. L., Mayol-Bracero, O. L., McMurry, P. H., Pauliquevis, T., Pöschl, U., Prather, K. A., Roberts, G. C., Saleska, S. R., Silva Dias, M. A., Spracklen, D. V., Swietlicki, E., and Trebs, I.: Sources and properties of Amazonian aerosol particles, Rev. Geophys., 48, RG2002, doi:10.1029/2008RG000280, 2010.

5 Matichuk, R. I., Colarco, P. R., Smith, J. A., and Toon, O. B.: Modeling the transport and optical properties of smoke aerosols from African savanna fires during the Southern African Regional Science Initiative campaign (SAFARI 2000), J. Geophys. Res., 112, D08203, doi:10.1029/2006JD007528, 2007.

Matichuk, R. I., Colarco, P. R., Smith, J. A. and Toon, O. B.: Modeling the transport and optical properties of smoke plumes from South American biomass burning, J. Geophys. Res., 113, D07208, doi:10.1029/2007JD009005, 2008.

10 McMeeking, G. R., Hamburger, T., Liu, D., Flynn, M., Morgan, W. T., Northway, M., Highwood, E. J., Krejci, R., Allan, J. D., Minikin, A., and Coe, H.: Black carbon measurements in the boundary layer over western and northern Europe, Atmos. Chem. Phys., 10, 9393-9414, https://doi.org/10.5194/acp-10-9393-2010, 2010.

Morello, T. F., Parry, L., Markusson, N. and Barlow, J.: Policy instruments to control Amazon fires: A simulation approach, Ecol. Econ., 138, 199-222, 2017.

15 Morgan, W. T., Allan, J. D., Bower, K. N., Highwood, E. J., Liu, D., McMeeking, G. R., Northway, M. J., Williams, P. I., Krejci, R., and Coe, H.: Airborne measurements of the spatial distribution of aerosol chemical composition across Europe and evolution of the organic fraction, Atmos. Chem. Phys., 10, 4065-4083, https://doi.org/10.5194/acp-10-4065-2010, 2010.

Morgan, W. T., Ouyang, B., Allan, J. D., Aruffo, E., Di Carlo, P., Kennedy, O. J., Lowe, D., Flynn, M. J., Rosenberg, P. D.,
20 Williams, P. I., Jones, R., McFiggans, G. B., and Coe, H.: Influence of aerosol chemical composition on N2O5 uptake: airborne regional measurements in northwestern Europe, Atmos. Chem. Phys., 15, 973-990, https://doi.org/10.5194/acp-15-973-2015, 2015.

Mu, M., Randerson, J. T., van der Werf, G. R., Giglio, L, Kasibhatla, P., Morton, D., Collatz, G. J., DeFries, R. S., Hyer, E. J., Prins, E. M., Griffith, D. W. T., Wunch, D., Toon, G. C., Sherlock V., and Wennberg, P. O.: Daily and 3-hourly
25 variability in global fire emissions and consequences for atmospheric model predictions of carbon monoxide, J. Geophys. Res., 116, D24303, doi: 10.1029/2011JD016245, 2011.

Ng , N. L., S. C. Herndon, A. Trimborn, M. R. Canagaratna, P. L. Croteau, T. B. Onasch, D. Sueper, D. R. Worsnop, Q. Zhang, Y. L. Sun and J. T. Jayne: An Aerosol Chemical Speciation Monitor (ACSM) for Routine Monitoring of the Composition and Mass Concentrations of Ambient Aerosol, Aerosol Sci. Technol., 45, 780-794, doi:
30 10.1080/02786826.2011.560211, 2011

Pereira, G., Siqueira, R., Rosário, N. E., Longo, K. L., Freitas, S. R., Cardozo, F. S., Kaiser, J. W., and Wooster, M. J.: Assessment of fire emission inventories during the South American Biomass Burning Analysis (SAMBBA) experiment, Atmos. Chem. Phys., 16, 6961-6975, https://doi.org/10.5194/acp-16-6961-2016, 2016.

Petters, M. D. and Kreidenweis, S. M.: A single parameter representation of hygroscopic growth and cloud condensation
35 nucleus activity, Atmos. Chem. Phys., 7, 1961-1971, doi:10.5194/acp-7-1961-2007, 2007.

Philip, S., R.V. Martin, J.R. Pierce, J.L. Jimenez, Q. Zhang, M.R. Canagaratna, D.V. Spracklen, C.R. Nowlan, L.N. Lamsal, M.J. Cooper and N.A. Krotkov: Spatially and seasonally resolved estimate of the ratio of organic mass to organic carbon, Atmos. Environ., 87, 34-40, 2014.

Pöschl, U., Martin, S. T., Sinha, B., Chen, Q., Gunthe, S. S., Huffman, J. A., Borrmann, S., Farmer, D. K., Garland, R. M.,
40 Helas, G., Jimenez, J. L., King, S. M., Manzi, A., Mikhailov, E., Pauliquevis, T., Petters, M. D., Prenni, A. J., Roldin, P., Rose, D., Schneider, J. , Su, H., Zorn, S. R., Artaxo, P. and Andreae, M. O.: Rainforest Aerosols as Biogenic Nuclei of Clouds and Precipitation in the Amazon, Science, 329, 1513-1516, 2010.

Randerson, J. T., Chen, Y., van der Werf, G. R., Rogers, B. M. and Morton, D. C.: Global burned area and biomass burning emissions from small fires, J. Geophys. Res., 117, G04012, doi:10.1029/2012JG002128, 2012.

Rap, A., C. E. Scott, D. V. Spracklen, N. Bellouin, P. M. Forster, K. S. Carslaw, A. Schmidt, and G. Mann: Natural aerosol direct and indirect radiative effects, Geophys. Res. Lett., 40, 3297-3301, doi: 10.1002/grl.50441, 2013.

Reddington, C. L., Butt, E. W., Ridley, D. A., Artaxo, P.,Morgan, W. T., Coe, H., and Spracklen, D. V.: Air quality and human health improvements from reductions in deforestation-related fire in Brazil, Nat Geosci., 8, 768-771, doi:10.1038/ngeo2535, 2015.

Reddington, C. L., Spracklen, D. V., Artaxo, P., Ridley, D. A., Rizzo, L. V., and Arana, A.: Analysis of particulate emissions from tropical biomass burning using a global aerosol model and long-term surface observations, Atmos. Chem. Phys., 16, 11083-11106, https://doi.org/10.5194/acp-16-11083-2016, 2016.

Reid, C.E., Brauer, M., Johnston, F.H., Jerrett, M., Balmes, J.R., Elliott, C.T.: Critical Review of Health Impacts of Wildfire Smoke Exposure, Environ. Health Perspect., 124, 1334-1343, 2016.

Scott, C. E., Rap, A., Spracklen, D. V., Forster, P. M., Carslaw, K. S., Mann, G. W., Pringle, K. J., Kivekäs, N., Kulmala, M., Lihavainen, H., and Tunved, P.: The direct and indirect radiative effects of biogenic secondary organic aerosol, Atmos. Chem. Phys., 14, 447-470, https://doi.org/10.5194/acp-14-447-2014, 2014.

Smith, L. T., Aragao, L., Sabel, C. E. and Nakaya, T.: Drought impacts on children's respiratory health in the Brazilian Amazon, Sci. Rep., 4, 2014.

Spracklen, D. V., Pringle, K. J., Carslaw, K. S., Chipperfield, M. P., and Mann, G. W.: A global off-line model of size-resolved aerosol microphysics: I. Model development and prediction of aerosol properties, Atmos. Chem. Phys., 5, 2227-2252, doi:10.5194/acp-5-2227-2005, 2005.

Stephens, M., Turner, N., and Sandberg, J.: Particle Identification by Laser-Induced Incandescence in a Solid-State Laser Cavity, Appl. Optics, 42, 3726, https://doi.org/10.1364/AO.42.003726, 2003.

Stockwell, C. E., Jayarathne, T., Cochrane, M. A., Ryan, K. C., Putra, E. I., Saharjo, B. H., Nurhayati, A. D., Albar, I., Blake, D. R., Simpson, I. J., Stone, E. A., and Yokelson, R. J.: Field measurements of trace gases and aerosols emitted by peat fires in Central Kalimantan, Indonesia, during the 2015 El Niño, Atmos. Chem. Phys., 16, 11711-11732, https://doi.org/10.5194/acp-16-11711-2016, 2016.

Stokes, R. H. and Robinson, R. A.: Interactions in aqueous nonelectrolyte solutions. I. Solute-solvent equilibria, J. Phys. Chem., 70, 2126-2130, 1966.

Thornhill, G. D., Ryder, C. L., Highwood, E. J., Shaffrey, L. C., and Johnson, B. T.: The effect of South American biomass burning aerosol emissions on the regional climate, Atmos. Chem. Phys., 18, 5321-5342, https://doi.org/10.5194/acp-18-5321-2018, 2018.

Tsigaridis, K., Daskalakis, N., Kanakidou, M., Adams, P. J., Artaxo, P., Bahadur, R., Balkanski, Y., Bauer, S. E., Bellouin, N., Benedetti, A., Bergman, T., Berntsen, T. K., Beukes, J. P., Bian, H., Carslaw, K. S., Chin, M., Curci, G., Diehl, T., Easter, R. C., Ghan, S. J., Gong, S. L., Hodzic, A., Hoyle, C. R., Iversen, T., Jathar, S., Jimenez, J. L., Kaiser, J. W., Kirkevåg, A., Koch, D., Kokkola, H., Lee, Y. H., Lin, G., Liu, X., Luo, G., Ma, X., Mann, G. W., Mihalopoulos, N., Morcrette, J.-J., Müller, J.-F., Myhre, G., Myriokefalitakis, S., Ng, N. L., O'Donnell, D., Penner, J. E., Pozzoli, L., Pringle, K. J., Russell, L. M., Schulz, M., Sciare, J., Seland, Ø., Shindell, D. T., Sillman, S., Skeie, R. B., Spracklen, D., Stavrakou, T., Steenrod, S. D., Takemura, T., Tiitta, P., Tilmes, S., Tost, H., van Noije, T., van Zyl, P. G., von Salzen, K., Yu, F., Wang, Z., Wang, Z., Zaveri, R. A., Zhang, H., Zhang, K., Zhang, Q., and Zhang, X.: The AeroCom evaluation and intercomparison of organic aerosol in global models, Atmos. Chem. Phys., 14, 10845-10895, https://doi.org/10.5194/acp-14-10845-2014, 2014.

Tsimpidi, A. P., Karydis, V. A., Pandis, S. N., and Lelieveld, J.: Global combustion sources of organic aerosols: model comparison with 84 AMS factor-analysis data sets, Atmos. Chem. Phys., 16, 8939-8962, https://doi.org/10.5194/acp-16-8939-2016, 2016.

Vakkari, V., J. P. Beukes, M. Dal Maso, M. Aurela, M. J. and P. G. van Zyl.: Major secondary aerosol formation in southern African open biomass burning plumes, Nat. Geosci., 11, 580-583, 2018.

van der Werf, G. R., Randerson, J. T., Giglio, L., Collatz, G. J., Mu, M., Kasibhatla, P. S., Morton, D. C., DeFries, R. S., Jin, Y., and van Leeuwen, T. T.: Global fire emissions and the contribution of deforestation, savanna, forest, agricultural, and peat fires (1997-2009), Atmos. Chem. Phys., 10, 11707-11735, doi:10.5194/acp-10-11707-2010, 2010.

5   van der Werf, G. R., Randerson, J. T., Giglio, L., van Leeuwen, T. T., Chen, Y., Rogers, B. M., Mu, M., van Marle, M. J. E., Morton, D. C., Collatz, G. J., Yokelson, R. J., and Kasibhatla, P. S.: Global fire emissions estimates during 1997–2016, Earth Syst. Sci. Data, 9, 697-720, https://doi.org/10.5194/essd-9-697-2017, 2017.

van Leeuwen, T. T., W. Peters, M. C. Krol, and G. R. van der Werf: Dynamic biomass burning emission factors and their impact on atmospheric CO mixing ratios, J. Geophys. Res. Atmos., 118, 6797-6815, doi: 10.1002/jgrd.50478, 2013.

10   van Leeuwen, T. T., van der Werf, G. R., Hoffmann, A. A., Detmers, R. G., Rücker, G., French, N. H. F., Archibald, S., Carvalho Jr., J. A., Cook, G. D., de Groot, W. J., Hély, C., Kasischke, E. S., Kloster, S., McCarty, J. L., Pettinari, M. L., Savadogo, P., Alvarado, E. C., Boschetti, L., Manuri, S., Meyer, C. P., Siegert, F., Trollope, L. A., and Trollope, W. S. W.: Biomass burning fuel consumption rates: a field measurement database, Biogeosciences, 11, 7305-7329, https://doi.org/10.5194/bg-11-7305-2014, 2014.

15   van Marle, M. J. E., R. D. Field, G. R. van der Werf, I. A. Estrada de Wagt, R. A. Houghton, L. V. Rizzo, P. Artaxo, and K. Tsigaridis: Fire and deforestation dynamics in Amazonia (1973–2014), Global Biogeochem. Cycles, 31, 24-38, doi: 10.1002/2016GB005445, 2017.

Wang, S. C. and Flagan, R. C.: Scanning electrical mobility spectrometer, Aerosol Sci. Tech., 13, 230-240, doi:10.1080/02786829008959441, 1990.

20   Weigum, N., Schutgens, N., and Stier, P.: Effect of aerosol subgrid variability on aerosol optical depth and cloud condensation nuclei: implications for global aerosol modelling, Atmos. Chem. Phys., 16, 13619-13639, https://doi.org/10.5194/acp-16-13619-2016, 2016.

Wiedinmyer, C., Akagi, S. K., Yokelson, R. J., Emmons, L. K., Al-Saadi, J. A., Orlando, J. J., and Soja, A. J.: The Fire INventory from NCAR (FINN): a high resolution global model to estimate the emissions from open burning,
25   Geosci. Model Dev., 4, 625-641, doi:10.5194/gmd-4-625-2011, 2011.

Yin, Y., et al.: Variability of fire carbon emissions in equatorial Asia and its nonlinear sensitivity to El Niño, Geophys. Res. Lett., 43, 10472-10479, doi:10.1002/2016GL070971, 2016.

Tables

	Annual emission (2002-2012 mean) (Gg a^{-1})			2012 / (2002-2012)	SAMBBA emission (Gg campaign^{-1})	
	OC	BC	OC:BC	OC+BC	OC	BC
Western Amazon (53-68°W, 1-12.5°S)						
GFAS	587	77.2	7.6	0.55	64.5	8.49
FINN	1480	163	9.1	0.80	241 [3.7]	26.6 [3.1]
GFED	692	81.0	8.5	0.92	134 [2.1]	15.6 [1.8]
Eastern Amazon (43-50°W, 4.5-15°S)						
GFAS	336	46.6	7.1	1.46	118	16.7
FINN	181	20.4	8.8	1.30	50.2 [0.4]	5.61 [0.3]
GFED	223	29.9	7.4	1.94	110 [0.9]	14.5 [0.9]

Table 1. Comparison of organic carbon (OC) and black carbon (BC) emissions from biomass burning in the GFASv1.2, FINNv1.5 and GFED4.1s emissions inventories. Emissions are summed separately for the western (53-68°W, 1-12.5°S) and eastern (43-50°W, 4.5-15°S) Amazon as shown in Fig. 2. Table reports long-term (2002-2012) mean annual total emissions, the ratio of annual total emissions in 2012 to the 2002-2012 mean and total emissions for the SAMBBA campaign period (13 September – 3 October 2012). All values are given to 3 significant figures. The ratios of total campaign emissions (FINN:GFAS and GFED:GFAS) are given in parentheses.

	noBBA	FINN	GFED	GFAS
Porto Velho, Phase 1				
PM2.5	-4.80	**-0.09**	-0.54	-1.35
Total mass	-3.43	0.45	**0.08**	-0.49
OA	-3.45	0.50	**0.11**	-0.50
BC	-53.12	**0.02**	-0.34	-1.32
Sulfate	**0.47**	2.69	2.32	1.96
Porto Velho, Phase 2				
PM$_{2.5}$	-2.26	0.32	**-0.25**	-0.61
Total mass	-0.72	1.94	0.89	**0.30**
OA	**-0.44**	2.44	1.18	0.47
BC	-34.63	**0.12**	-0.51	-1.51
Sulfate	**-0.06**	2.22	1.51	1.24

Table 2. Summary of comparison between model and ground-based *in-situ* observations at the Porto Velho measurement station expressed as normalised mean bias factor (NMBF). Values are shown for PM2.5 (particulate matter with diameters smaller than 2.5 µm), total mass (mass measured by the ACSM plus equivalent black carbon measured by the aethelometer), organic aerosol (OA), black carbon (BC) and sulfate. Values are shown for the model with FINN1.5, GFAS1.2, GFED4.1s emissions and with no biomass burning emissions (noBBA). The numbers highlighted in bold show the model simulation with the smallest bias.

	noBBA	FINN	GFED	GFAS
Western Amazon, Phase 1				
OA (<2.5 km)	-7.39	**-0.33**	-0.97	-1.96
BC (<2.5 km)	-35.88	**-0.01**	-0.51	-1.32
Sulfate (<2.5 km)	-2.04	**-0.38**	-0.63	-0.77
AOD550 (MODIS)	-5.13	**-0.96**	-1.47	-1.81
AOD500 (AERONET)	-7.06	**-0.56**	-0.59	-1.31
Western Amazon, Phase 2				
OA (<2.5 km)	-1.12	1.21	0.41	**0.03**
BC (<2.5 km)	-20.94	0.56	**-0.06**	-0.56
Sulfate (<2.5 km)	-0.64	0.68	0.37	**0.22**
AOD550 (MODIS)	-4.10	**-1.02**	-1.37	-1.63
AOD500 (AERONET)	-4.84	**-0.43**	-0.77	-1.15
Eastern Amazon				
OA (<4 km)	-13.21	-2.78	-1.08	**-0.92**
BC (<4 km)	-42.05	-5.55	-1.75	**-1.41**
Sulfate (<4 km)	**0.30**	0.72	1.45	1.24
AOD550 (MODIS)	-4.92	-2.41	-1.44	**-1.23**

Table 3. Summary of comparison between model and observations. Comparisons are shown for observations from the aircraft: organic aerosol (OA), black carbon (BC), sulfate mass concentrations; satellite: aerosol optical depth at 550 nm (AOD550) from MODIS, and AOD500 from AERONET. Comparisons are expressed as normalised mean bias factor (NMBF, blue indicates model underestimation). Aircraft comparisons are for concentrations below 2.5 km (western Amazon) or 4 km (eastern Amazon). AERONET comparisons are the average NMBF across 5 stations. Values are shown for the model with FINN1.5, GFAS1.2, GFED4.1s emissions and with no biomass burning emissions (noBBA). The numbers highlighted in bold show the model simulation with the smallest bias.

Figures
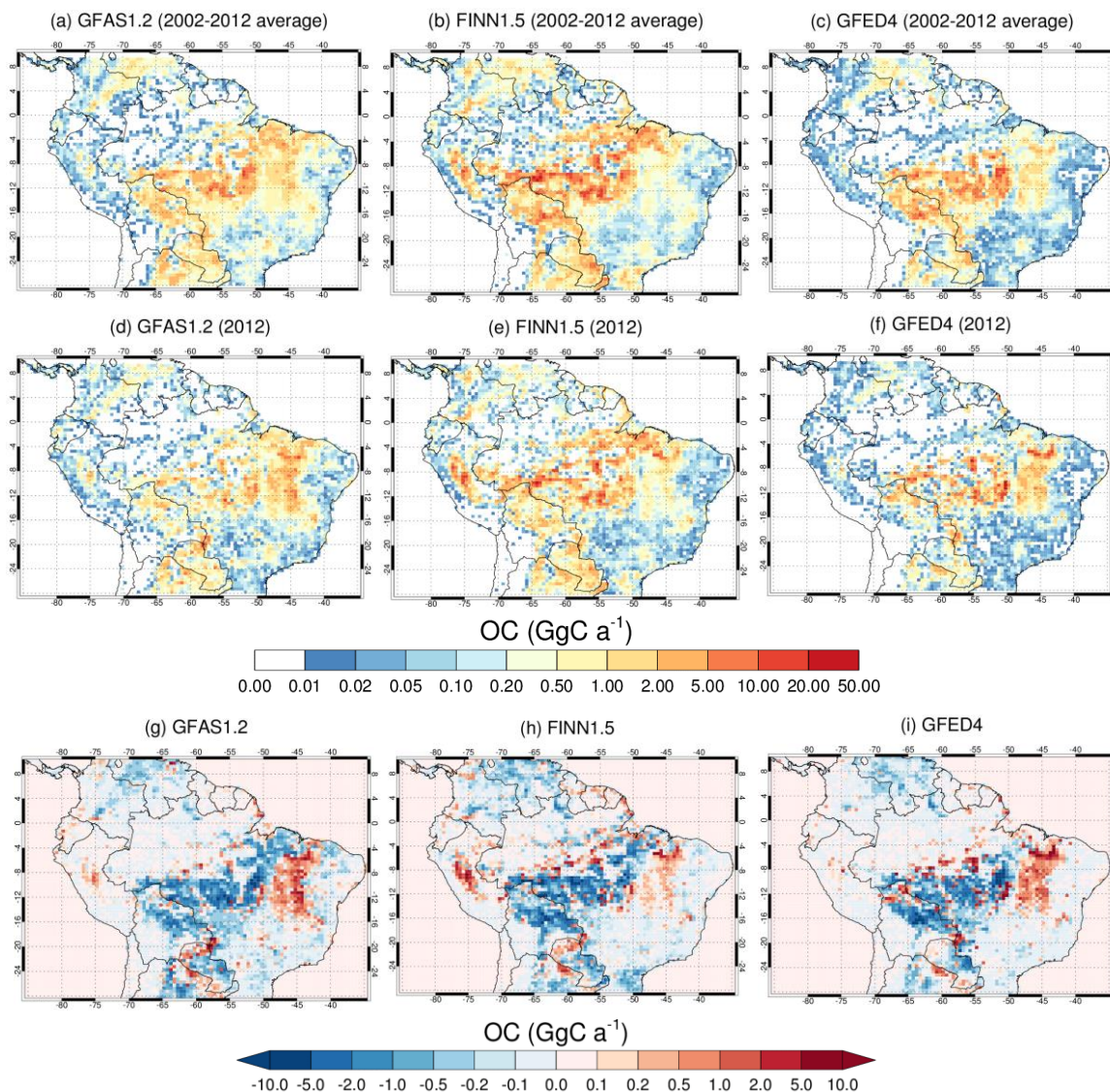
Figure 1. Maps of estimated total annual organic carbon (OC) aerosol emissions from fire shown as **(a)**-**(c)** an average for the period 2002 to 2012 and **(d)**-**(f)** for 2012. The difference in OC emissions between 2012 and 2002 to 2012 (2012 emissions minus 2002-2012 average) is shown in **(g)**-**(i)**. Blue colours show where emissions in 2012 were less than in 2002 to 2011, while red colours show where emissions were greater. Emissions are shown for GFAS version 1.2 (left) and FINN version 1.5 (middle) and GFED version 4 (right).
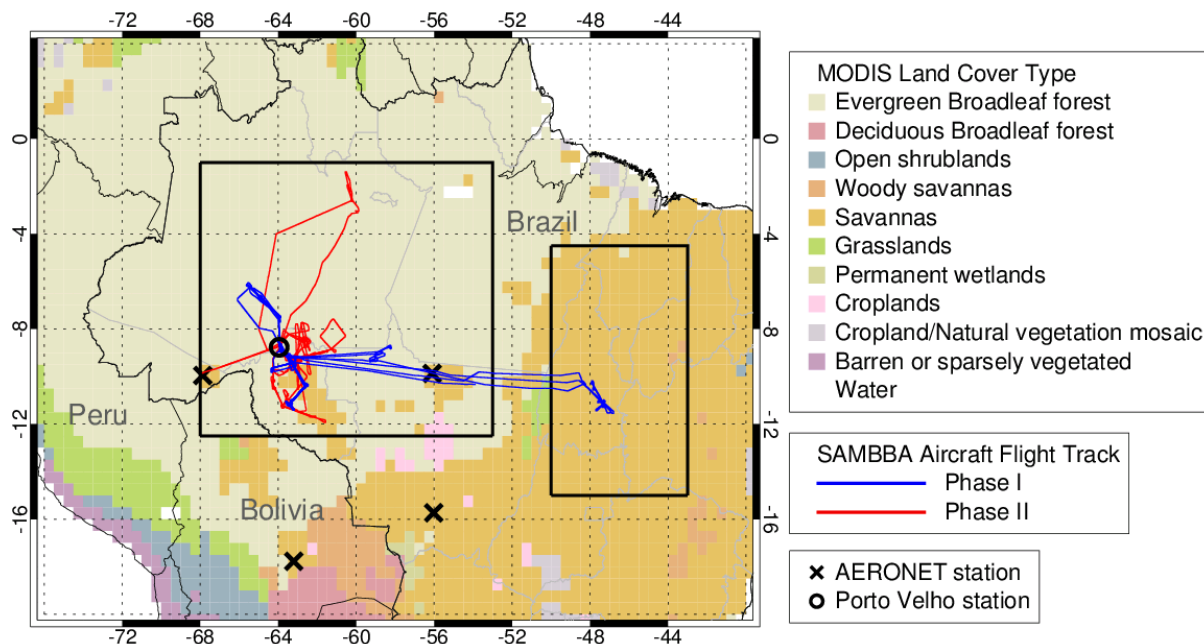
Figure 2. Flight tracks of the FAAM aircraft during the SAMBBA field campaign (Phase 1: 13 - 23 September; Phase 2: 23 September – 3 October 2012). The location of the Porto Velho ground station is shown by a black circle. The locations of AERONET stations operating during the SAMBBA campaign are shown by black crosses: Porto Velho UNIR (63.94°W, 8.84°S), Alta Floresta (56.10°W, 9.87°S), Rio Branco (67.87°W, 9.96°S), Cuiaba-Miranda (56.02°W, 15.73°S), Santa Cruz UTEPSA (63.20°W, 17.77°S). The eastern (43-50°W, 4.5-15°S) and western (53-68°W, 1-12.5°S) domains are shown with black boxes. Land cover type is shown using the standard MODIS land cover type data product (MCD12Q1) in the IGBP Land Cover Type Classification (Channan et al., 2014; Friedl et al., 2010).
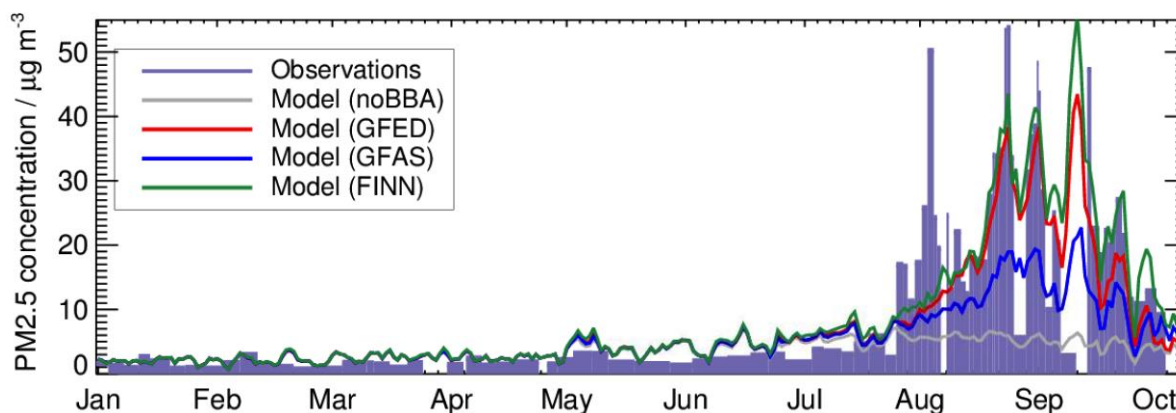
Figure 3. Time series of simulated (lines) and observed (bars) PM2.5 concentrations at Porto Velho between January and November 2012. Simulated daily mean concentrations are shown with FINN1.5 (green), GFAS1.2 (blue), GFED4 (red) emissions and with no biomass burning emissions (grey). Observed PM2.5 concentrations are averages over sampling periods that ranged from <1 day to 7 days in 2012. The NMBF values are given separately for Phase 1 and Phase 2 of the SAMBBA field campaign in Table 2.

(a)

(b)
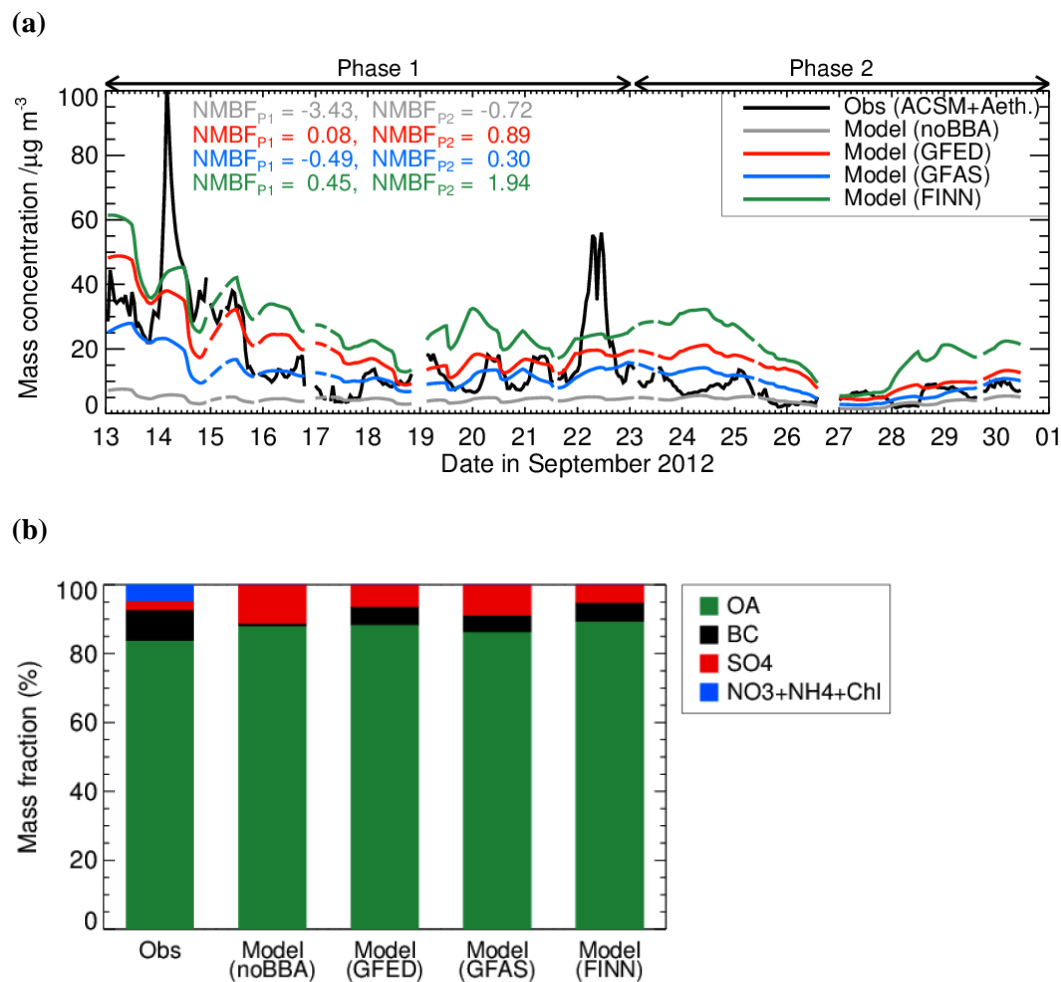
Figure 4. Composition resolved aerosol mass at Porto Velho during the SAMBBA campaign. **(a)** Time series of observed (black) and simulated (colour) total aerosol mass. The observed aerosol mass is the total mass from the ACSM plus equivalent BC from the aethelometer. Simulated total aerosol mass is shown for the model with FINN1.5 (green), GFAS1.2 (blue), GFED4 (red) emissions and with no biomass burning emissions (noBBA; grey). Numbers on the panel show the NMBF for the SAMBBA campaign separately for Phase 1 (P1) and Phase 2 (P2) (also see Table 2). **(b)** Bar chart showing observed and simulated average aerosol composition during the campaign: black carbon (BC; black), nitrate+ammonium+chloride (NO3+NH4+Chl; blue, not treated by the model), organic aerosol (OA; green) and sulfate (SO4; red).
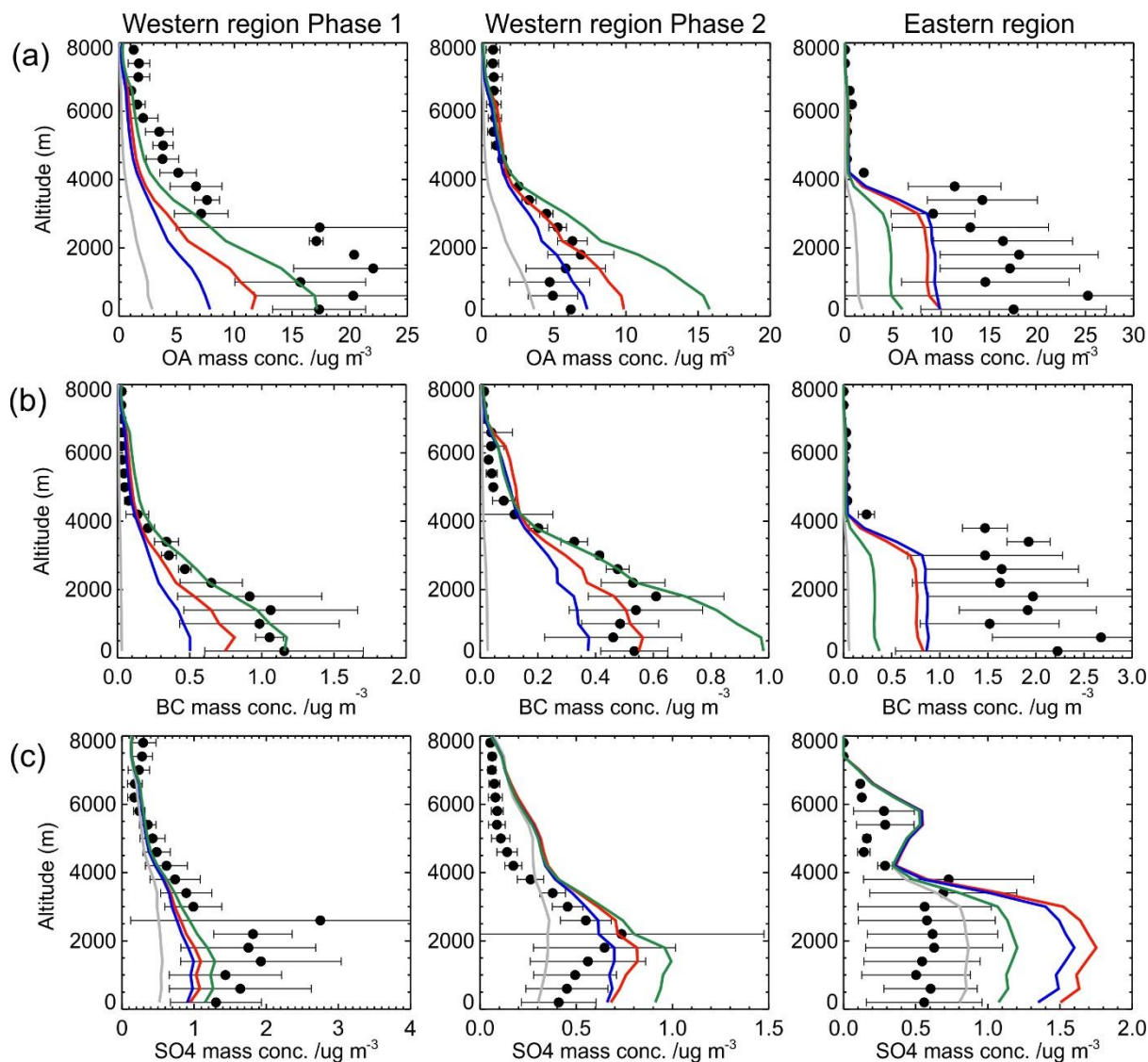
Figure 5. Mean observed and simulated vertical profiles of **(a)** organic aerosol (OA), **(b)** black carbon (BC) and **(c)** sulfate (SO4) during the SAMBBA aircraft campaign, sectioned into 400 m altitude bins. Observations are shown by the black data points; simulated concentrations are shown for the model with FINN1.5 (green), GFAS1.2 (blue), GFED4 (red) emissions and with no biomass burning emissions (grey). The simulated data (linearly interpolated to the flight track of the aircraft) and the observations are split into western and eastern regions of the Amazon (Fig. 2) and by time (Phase 1: 13/09/2012 – 22/09/2012, Phase 2: 23/09/2012 - 03/10/2012) for the western region. Error bars show the standard deviation of the observed mean. Concentrations are reported at STP conditions (at 273.15 K and 1013.25 hPa). The NMBF values are given separately for the western region (Phase 1 and Phase 2) and eastern region in Table 3.
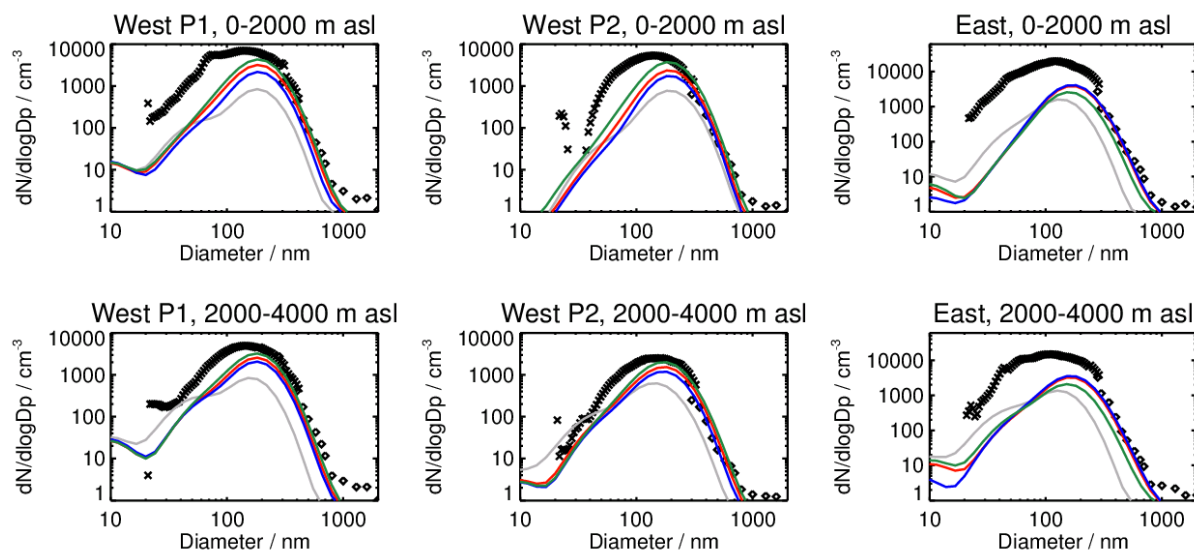
Figure 6. Mean observed (black) and simulated (colour) aerosol number size distributions during the SAMBBA aircraft campaign for two altitude bands: between the surface and 2 km (top panel) and between 2 and 4 km asl (bottom panel). The observed number size distribution was measured with Scanning Mobility Particle Sizer (black crosses) and a Grimm optical particle counter (black diamonds). The simulated data (linearly interpolated to the flight track of the aircraft) and the observations are split into western and eastern regions of the Amazon (Fig. 2) and by time (P1: 13/09/2012 – 22/09/2012, P2: 23/09/2012 - 03/10/2012) for the western region. Simulated concentrations are shown for the model with FINN1.5 (green), GFAS1.2 (blue), GFED4 (red) emissions and with no biomass burning emissions (grey).
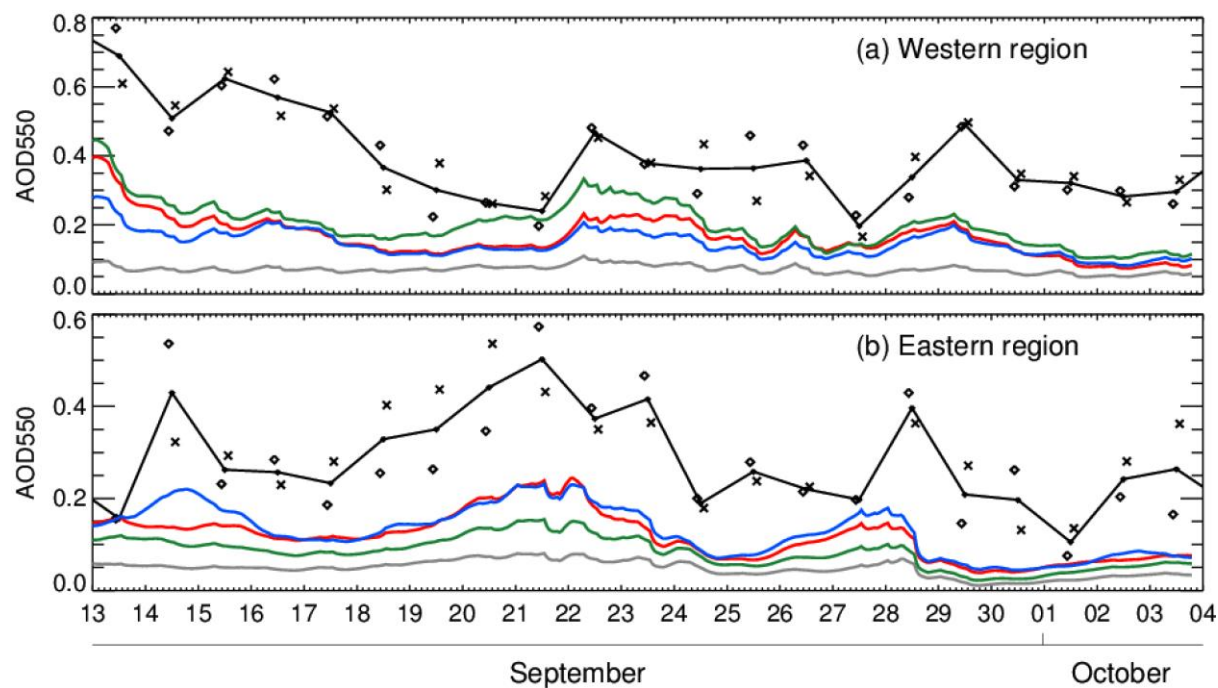
Figure 7. Time series of simulated (colour) and observed (black) aerosol optical depth at 550 nm (AOD550) for the SAMBBA campaign (13 September – 3 October 2012) over **(a)** the western Amazon (53-68°W, 1-12.5°S) and **(b)** the eastern Amazon (43-50°W, 4.5-15°S). Observed AOD550 retrieved by MODIS on-board Terra (over pass time: 10:30 local time) is shown by the black diamonds and AOD550 retrieved by MODIS on-board Aqua (over pass time: 13:30 local time) is shown by the black crosses; the black line shows an average value for each day (plotted at midday local time). Simulated hourly AOD550 (plotted at local time for Rondônia, Brazil. UTC-4h) is shown for the model with FINN1.5 (green), GFAS1.2 (blue), GFED4 (red) emissions and with no biomass burning emissions (grey). The NMBF values are given separately for the western region (Phase 1 and Phase 2) and eastern region in Table 3.
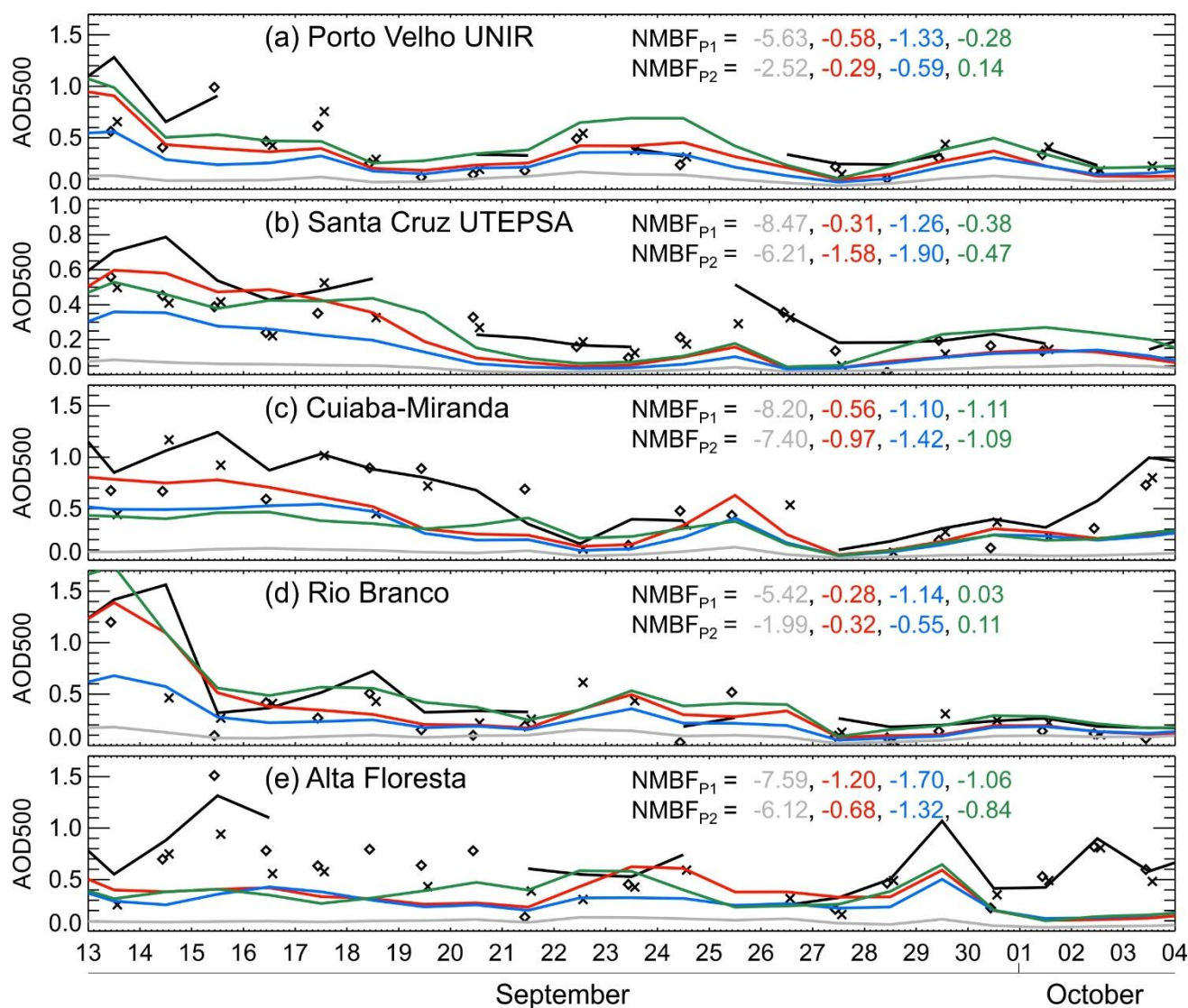
Figure 8. Time series of simulated (colour) and observed (black) daily aerosol optical depth (AOD) during the SAMBBA campaign at 5 AERONET stations in the western and southern Amazon: **(a)** Porto Velho UNIR (63.94°W, 8.84°S), **(b)** Santa Cruz UTEPSA (63.20°W, 17.77°S), **(c)** Cuiaba-Miranda (56.02°W, 15.73°S), **(d)** Rio Branco (67.87°W, 9.96°S) and **(e)** Alta Floresta (56.10°W, 9.87°S). Daily mean AOD at 500 nm (AOD500) from AERONET (black line) is compared to AOD550 retrieved by MODIS (Terra: black diamonds; Aqua: black crosses), using grid cells nearest the AERONET station location. Simulated daily mean AOD500 is shown for the model with FINN1.5 (green), GFAS1.2 (blue), GFED4 (red) emissions and with no biomass burning emissions (purple). The NMBF values are given separately for Phase 1 (P1) and Phase 2 (P2) of the campaign.